Research on measurement of thickness and refractive index of glass plates with a spectrally resolved interferometer

Doctoral Program of Electrical and Information Engineering
Graduate School of Science and Technology
Niigata University

ZHANG Kaining

July 2022

ABSTRACT

Spectral resolved interferometer (SRI) has a broadband light source and a spectrum analyzer (SPA). The interference signal produced by the SPA is roughly expressed by $\cos(2\pi\nu L)$, where ν is wavenumber and L is an optical path difference (OPD) between an object surface and an reference surface. When L is large, a high-resolution SPA is needed. A SPA with a wavelength resolution higher than about 0.05 nm is required to measure a large thickness more than a few millimeters. In this thesis a new method is proposed to measure a large thickness of glass plate by using a SPA with a low-resolution of 0.5 nm and a piezo electric transducer (PZT) stage with a positioning accuracy of 10 nm. The position of a reference surface in the SRI of Michelson type is adjusted by the PZT stage to generate a small OPD. Thus, the interference signal can be detected with the low-resolution SPA. There are two ways to extract the OPD L from the detected interference signal. One way is that L is obtained from a position of maximum amplitude in Fourier transform of the interference signal. The other way is that L is obtained from the spectral phase $2\pi\nu L$ which is extracted through Fourier transform and frequency filtering. When the object is a glass plate, OPD L is a function of wavenumber ν due to the phase refractive index $n(\nu)$ of a glass plate. This phenomenon is called “dispersion effect”. OPD L cannot be exactly obtained from a position of the maximum amplitude because of a strong dispersion effect when thickness T of a glass plate is large. On the other hand, OPD L can be exactly obtained from the spectral phase because L is directly related with the spectral phase and the dispersion effect produces only nonlinear component in the spectral phase. Hence, in this thesis spectral phase is utilized to measure thickness T and refractive index $n(\nu)$.There is another dispersion effect caused by a beam splitter cube whose two sides do not have the same length. In order to eliminate this dispersion effect and measure thickness T, different optical configurations of the SRI are formed by using another fixed reference surface in the object arm or a compensation glass (CG) plate in the reference arm. Different spectral phases are detected with different positions of the reference surface in the different optical configurations. Thickness T can be measured from many detected spectral phases. Measurement of phase refractive index of a glass plate can be achieved by using the SRI and the measurement method in the thickness measurement. The following three different measurements are described in this thesis.

(1) Large thickness measurement of glass plate whose refractive index is not known.

Amplitude distribution in Fourier transform of an interference signal produced by a rear surface of glass plate has a large spread width due to the dispersion effect of the glass plate. The position of the reference surface is adjusted so that the interference signal having a small OPD can be detected with the low-resolution SPA. Another reference surface is fixed in the object arm. Four different optical configurations are used with four different positions of the reference surface. From the four different spectral phases a spectral phase without containing the refractive index of glass plate is derived. The thickness of the glass plate can be measured from the slope of this spectral phase

distribution. In experiments, it was confirmed that the detected position of maximum amplitude in Fourier transform of the interference signal agreed with the theoretical one. A small measurement error of 50 nm was achieved in measuring 1 mm thickness of a glass plate.

(2) More larger thickness measurement of glass plate using a compensation glass whose refractive index is known.

In order to reduce the large spread width in the amplitude distribution caused by the dispersion effect of a larger thickness, a compensation glass (CG) plate is employed. Thickness larger than one millimeter can be measured by using the CG. A spectral phase is detected from the interference signal generated from the front surface of a glass plate and a reference surface. After putting the CG into the reference arm, another spectral phase is detected from an interference signal generated from the rear surface of the glass plate and the reference surface. A detected spectral phase is obtained from these two spectral phases. By comparing the nonlinear component of the detected spectral phase with a theoretical one, the difference in thickness between the glass plate and the CG can be obtained. Thickness of the glass plate can be measured from this thickness difference and a linear component of the detected spectral phase. In experiments, measurement errors were less than 800 nm and 2 μm for 1 mm and 5 mm-thickness glass plates, respectively.

(3) Phase refractive index measurement of glass plate together with thickness measurement.

Phase refractive index is an important property of optical material. The SRI and the measurement method in the thickness measurement are applied for measurement of phase refractive index. Object was a quartz glass plate with 20 μm thickness. By combining the three spectral phases detected in two different configurations, thickness of the quartz glass was measured with an error less than 6 nm. The refractive index is obtained from one of the three spectral phases. It is required to determine 2π phase ambiguity existing in the spectral phase distribution for the refractive index measurement. This determination is carried out by fitting the spectral phase distribution with fitting functions based on Cauchy dispersion formula. Phase refractive index distribution of the quartz glass plate could be measured with an error less than 0.0005 from the measured thickness, the determined 2π phase ambiguity, and the spectral phase distribution.

CONTENT

CHAPTER 1

INTRODURCTION

1.1. Interferometers

1.1.1. Single wavelength interferometer

Interferometry is an established technique which has been applied for many kinds of optical measurements. Michelson type interferometer [C1.1] is a well-known one, and it is utilized widely to generate interference signals. Basic principle of interferometer with a single wavelength light source is explained with a Michelson type interferometer shown in Fig. 1.1. A single wavelength of the light source is λ_O. A beam from light source is divided by a beam splitter (BS). One beam is reflected by an object surface, and another beam is reflected by a reference surface. These two beams are combined again by the BS. The interference signal between these two beams is detected with a detector. The position of object surface is Z_O, and the position of reference surface is Z_R. Optical path difference (OPD) between these two beams is equal to $L=2(Z_O-Z_R)$. The interference signal is expressed as $S=\cos[(2\pi/\lambda_O)L]=\cos[(2\pi/\lambda_O)2(Z_O-Z_R)]$ by ignoring constant terms. When the position of object surface changes from Z_O to Z_O+h as shown in Fig. 1.1, the interference signal becomes $S(h)=\cos[(2\pi/\lambda_O)2(Z_O+h-Z_R)]$. Measurement of

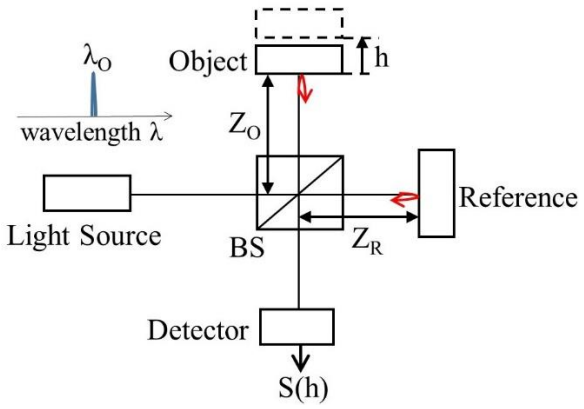

Fig. 1.1. Configuration of Michelson interferometer.

the displacement h is made by observing the signal $S(h)$. Figure 1.2 shows $S(h)=\cos[(4\pi/\lambda_O)h)]$ along h, where it is assumed that $S(0)=1$ at $h=0$. After a displacement h, $S(0)=1$ changes to $S(h)=A$. Then the displacement h is regarded as h_1 or h_2. And $h=h_1<\lambda_O/4$ and $h=h_2>\lambda_O/4$ cannot be distinguished by the change in the $S(h)$. Hence there is uncertainness in this measurement

and the measurable range is $\lambda_O/4$. This uncertainness is generally called phase ambiguity. Therefore, white light source is used to overcome the phase ambiguity produced by single wavelength light source.

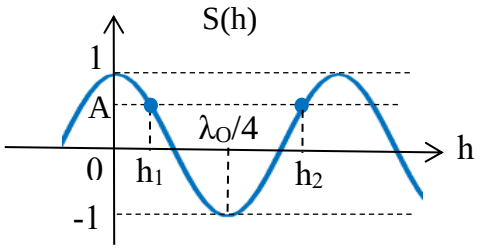

Fig. 1.2. Interference signals generated by single wavelength λ_O.

1.1.2. White-light scanning interferometer

In order to solve the measurable range of $\lambda_O/4$ described in section 1.1.1, white-light scanning interferometer (WLSI) [C1.2] is used. Configuration of WLSI is shown in Fig. 1.3. White light source has a broad spectrum that continuously distributes along wavelength axis. A BS divides a beam from a white light source for object and reference arms. The beams reflected from the two arms are combined again to generate the interference signal $S(Z_R)$. The position Z_R of reference surface is scanned with a PZT stage. A successive signal of $S(Z_R)$ along the scanning position is detected with a detector. It is

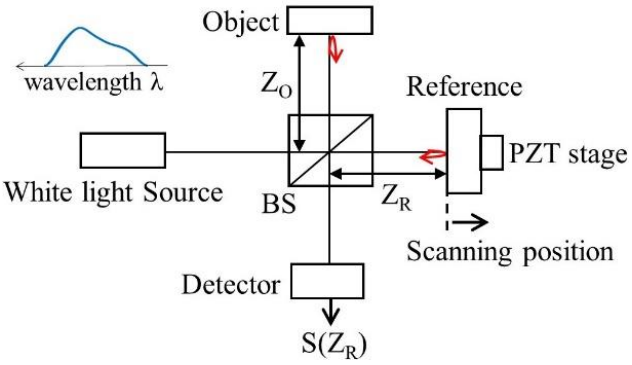

Fig. 1.3. White-light scanning interferometer.

regarded that the broad spectrum of white light source consists of multiple wavelengths of λ_i and each wavelength produces an interference signal of $S_{\lambda i}(Z_R)=\cos[(2\pi/\lambda_i)L]=\cos[(2\pi/\lambda_i)2(Z_O-Z_R)]$ as described in Sec. 1.1.1. Figure 1.4 shows schematically how a white-light scanning interference signal $S(Z_R)$ is generated from the interference signals $S_{\lambda i}(Z_R)$ produced by a single wavelength λ_i. The interference signal $S(Z_R)$ is generated by summing all of $S_{\lambda i}(Z_R)$ together. The summation of waveforms of $S_{\lambda i}(Z_R)$ results in

constructive and destructive effects on the magnitude of $S(Z_R)$ along Z_R. Since all of the waveforms of $S_{\lambda i}(Z_R)$ have a peak value of 1 at $Z_R=Z_O$, a large peak of $S(Z_R)$ appears at $Z_R=Z_O$ or $L=0$. This peak is larger than all of other peaks where constructive effect occurs in the summation. The position of the peak provides a measurement value of Z_O. Thus, a large value Z_O of object position

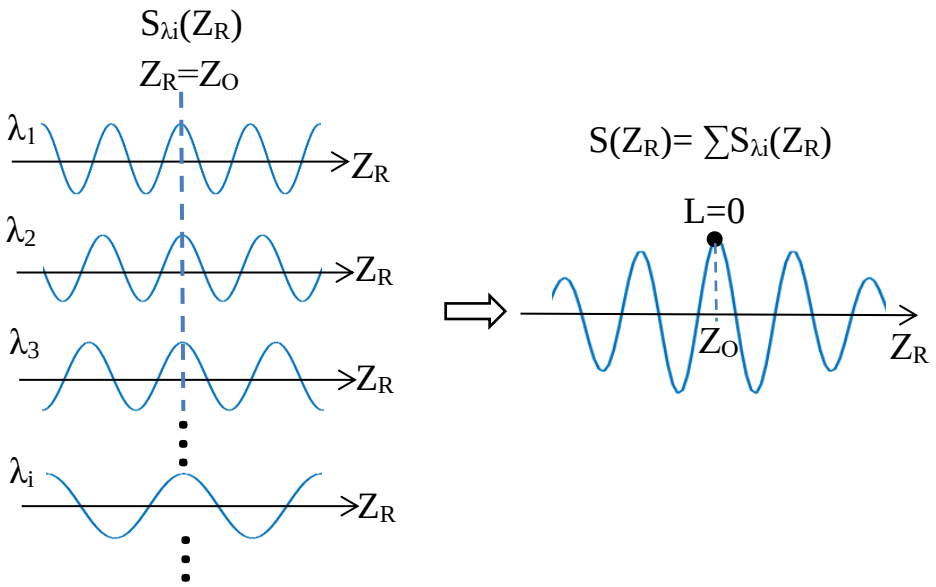

Fig. 1.4. Distributions of whit-light scanning interferometer.

can be measured, and the measurable range of WLSI is extended compared with single wavelength interferometer. Here exact scanning position is important for the measurement of object position because Z_O is decided by the value of Z_R which provides a maximum value in $S(Z_R)$. The measurement accuracy depends on an unstable scanning speed of the PZT stage movement. Hence, another interferometer using a white light source without the scanning of reference position is required. This interferometer is spectrally resolved interferometer described in the next section.

1.1.3. Spectrally resolved interferometer (SRI)

Figure 1.5 shows a schematic configuration of SRI with a white light source. A beam from light source is divided by a BS. The beams reflected from object and reference are combined again by the BS, and interference signal is detected with a spectrum analyzer (SPA) [C1.3]. Generally, SPA consists of a diffraction grating, a collimating lens (CL), and a line CCD. The white light contains multiple wavelengths of $\lambda_1,..,\lambda_i,..,$ and the beams of the wavelengths are separated by the diffraction grating. An interference intensity distribution along $\lambda_1,..,\lambda_i,..$ is detected with the line CCD, and the output of the CCD is an

spectrally resolved interference signal. The interference signal is given by $S(\lambda)=I(\lambda)+I(\lambda)\cos[4\pi(Z_O-Z_R)/\lambda]$, where $I(\lambda)$ is the spectrum intensity of light source. The OPD of $L=2(Z_O-Z_R)$ containing in $S(\lambda)$ is the value to be measured. One method to extract L from

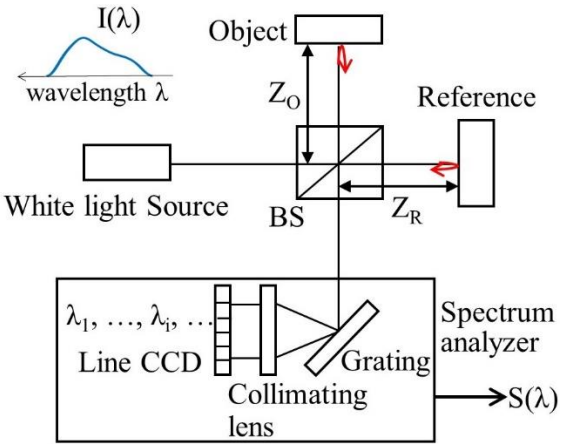

Fig. 1.5. Configuration of spectrally resolved interferometer (SRI).

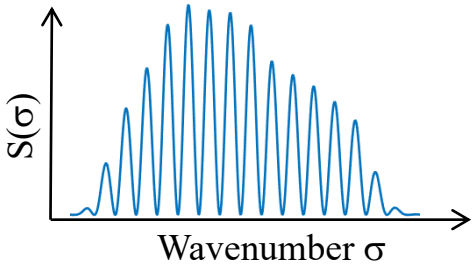

Fig. 1.6. Spectrally resolved interference signal S(σ).

$S(\lambda)$ is to use Fourier transform of $S(\lambda)$. For performing Fourier transform, the detected interference signal $S(\lambda)$ is converted to an interference signal $S(\sigma)=I(\sigma)+I(\sigma)\cos(2\pi L\sigma)$, where $\sigma=1/\lambda$ is wavenumber. Figure 1.6 shows a spectrally resolved interference signal $S(\sigma)$. Fourier transform is performed between two domains of σ and $d=2L$. The amplitude distribution $|F(d)|$ of

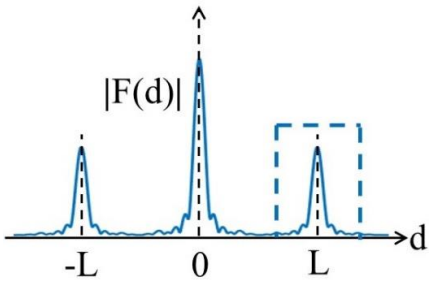

Fig. 1.7. Amplitude distribution of $F(d)$.

Fourier transform of $S(\sigma)$ is shown in Fig. 1.7. The distribution has three peaks at d=-L, 0, L. The position of one peak provides a measurement value of L=2(Z_O-Z_R).

Another method to extract L from $S(\lambda)$ is to extract the phase term of $2\pi L\sigma$ containing in $S(\sigma)$. The frequency component of $F(d)$ at d=L is selected by a rectangular window as shown in Fig. 1.7. Inverse Fourier transform is performed on this windowed distribution. The phase distribution calculated through Fourier transform is wrapped in the region of 2π. The wrapped phase distribution of $2\pi L\sigma$ is unwrapped to obtain a continuous phase distribution of $\varphi(\sigma)=2\pi L\sigma+2\pi p$, where p is an integer and an ambiguous value. The distribution of $\varphi(\sigma)$ is called spectral phase. Thus a measurement value of L can be obtained from the slope of spectral phase as $L=\{d[\varphi(\sigma)]/d\sigma\}/2\pi$. When random phase noise is contained in $\varphi(\sigma)$, the measurement value provided by the slope of $\varphi(\sigma)$ is not sensitive to random phase noise. Therefore, this measurement value is more exact than that provided by $|F(d)|$. The spectral phase is utilized in this thesis for measurements of thickness and refractive index.

1.2. Motivation

1.2.1. Thickness measurement by SRI

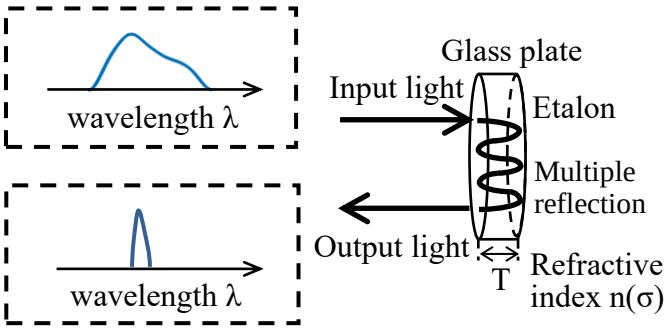

Fig. 1.8. Importance of thickness measurement.

Glass plates are important components in optical devices such as an etalon shown in Fig. 1.8. An input light with a broad spectrum is converted into a narrow spectrum light by multiple reflections. This narrow spectrum is determined by the thickness T and the refractive index $n(\lambda)$ of glass plate. Thus, thickness measurement of T is required. This measurement can be achieved with SRI and WLSI. Although the measurement region of SRI is limited to one point or one line, SRIs have been widely used for thickness measurement [C1.4-C1.5] because the configuration of SRI is very simple compared to that of WLSI.

1.2.1.1. Variable position of reference surface and low-resolution SPA

A SRI shown in Fig. 1.9 is used for thickness measurement. An input beam is divided by a BS for the object and reference arms. Object is a glass plate with thickness T and refractive index $n(\sigma)$. A reference surface is fixed on a PZT stage. When the position of reference surface is Z_R, an interference signal between the two beams from the front surface of object and the reference surface is expressed as $S_F(\sigma)=I(\sigma)+I(\sigma)\cos(2\pi L_F\sigma)$, where $L_F=2(Z_O-Z_R)$. An interference signal between the two beams from the rear surface of object and the reference surface is expressed as $S_R(\sigma)=I(\sigma)+I(\sigma)\cos(2\pi L_R\sigma)$, where $L_R=2(Z_O+n(\sigma)T-Z_R)=L_F+2n(\sigma)T$.

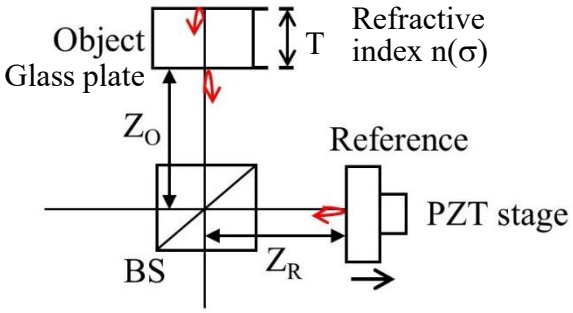

Fig. 1.9. Interference signals produced from a glass plate.

Figure 1.10 shows these two interference signals. Period of the waveform of the signal $S_F(\sigma)$ is large due to L_F=10 μm. On the other hand, the signal $S_R(\sigma)$ has a small period due to a large value of L_R and its waveform is not shown clearly. When T=1 mm and the value of $n(\sigma)$ is regarded as a constant value of 1.515, the large value of L_R becomes 3040 μm. A high resolution SPA is required to detect this $S_R(\sigma)$. High resolution SPA is expensive and the size is large. Thus, in this thesis a measurement method is proposed to

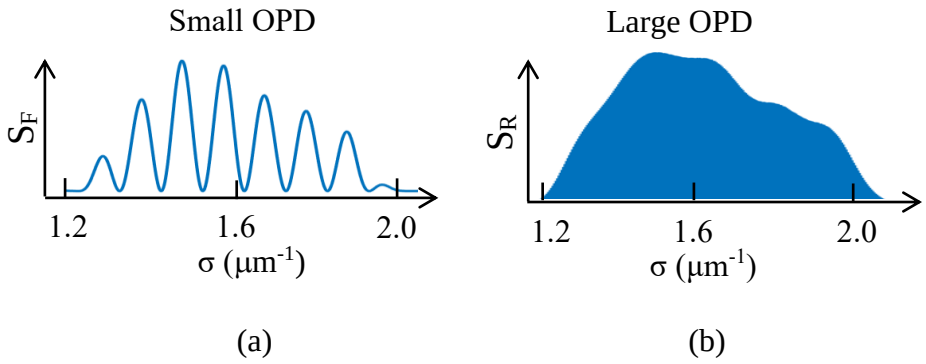

Figure 1.10. Distributions of (a) $S_F(\sigma)$ and (b) $S_R(\sigma)$. (a) Small OPD of L_F=10 μm, and (b) large OPD of L_R=3040μm at $n(\sigma)$=1.515.

detect $S_R(\sigma)$ with a low resolution SPA. In this method the position Z_R of reference surface is changed with a PZT stage so that a small L_R is produced. When the position Z_R is changed by 1495 μm, a small value of L_R is obtained as L_R=50 μm at $n(\sigma)$=1.515. Figure 1.11 shows the distribution of $S_R(\sigma)$ at the small L_R. This $S_R(\sigma)$ can be detected with a SPA of about 0.5 nm resolution. Therefore, the variable reference position enables to detect the interference signal with a low resolution SPA even when thickness T of an object is large.

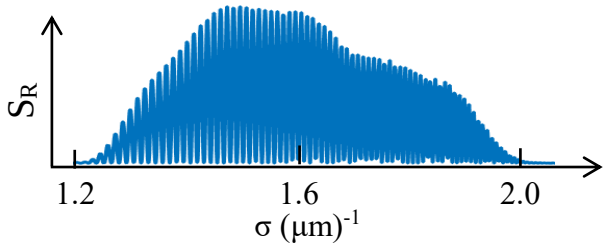

Fig. 1.11. Distribution of $S_R(\sigma)$ where L_R=50 μm at $n(\sigma)$=1.515.

1.2.1.2. Spectral phase

Since the refractive index of $n(\sigma)$ increases with increase of σ, the OPD of $L_R = L_F + 2n(\sigma)T$ is not a constant value although L_F is a constant value. Figure 1.12 shows the amplitude distribution $|F_F(d)|$ and $|F_R(d)|$ of Fourier transform of the interference signals $S_F(\sigma)$ of Fig. 1.10 (a) and $S_R(\sigma)$ of Fig. 1.11. The distribution of $|F_R(d)|$ has a wide spread because of the non-constant value of L_R. This phenomena is called dispersion effect.

The constant value of L_F can be obtained by the peak position of $|F_F(d)|$ because $S_F(\sigma)$ has no dispersion effect. The spread width of $|F_R(d)|$ is large and the peak position of $|F_R(d)|$ is not pronounced due to the dispersion effect of $n(\sigma)T$. Moreover the peak position does not have a clear relation with the non-constant value L_R. On the other hand, the phase term containing in $S_R(\sigma)$ is extracted through Fourier transform to obtain the distribution of L_F. The extracted spectral phase is expressed as $\varphi_R(\sigma)=4\pi(Z_O+n(\sigma)T-Z_R)\sigma$. Although the distribution of $\varphi_R(\sigma)$ is not a linear line due to $n(\sigma)T$, a least square linear line of $\varphi_R(\sigma)$ provides a value of T which is more exact than that obtained from the peak position of $|F_R(d)|$. Since the spectral phase is directly related with OPD, it will provide useful information such as thickness T and refractive index $n(\sigma)$ about object. Therefore, in this thesis the spectral phase is utilized for thickness and refractive index measurements.

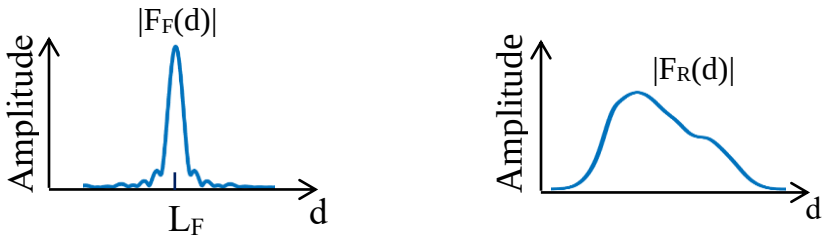

Fig. 1.12. Amplitude of $|F_F(d)|$ and $|F_R(d)|$.

1.2.1.3. Elimination of dispersion effect by BS

It was made clear in experiments that the BS do not have the same length in the two sides of the cube [C1.6], and this length difference is denoted as l_ε. Dispersion effect generated by the BS is expressed as $n_B(\sigma)l_\varepsilon$, where $n_B(\sigma)$ is the refractive index of BS. In this case, spectral phase $\varphi_F(\sigma)$ of the interference signal $S_F(\sigma)$ contains the term of $n_B(\sigma)l_\varepsilon$. Spectral phase $\varphi_R(\sigma)$ of $S_R(\sigma)$ contains the terms of $n_B(\sigma)l_\varepsilon$ and $n(\sigma)T$. Distributions of $\varphi_F(\sigma)$ and $\varphi_R(\sigma)$ are shown in Fig. 1.13. Since both $\varphi_F(\sigma)$ and $\varphi_R(\sigma)$ contain the term of $n_B(\sigma)l_\varepsilon$, the dispersion effect generated by BS is eliminated in $\varphi_S(\sigma)=\varphi_R(\sigma)-\varphi_F(\sigma)$ as shown in Fig. 1.13. Therefore, dispersion effect due to the BS can be eliminated by subtraction between two different spectral phases.

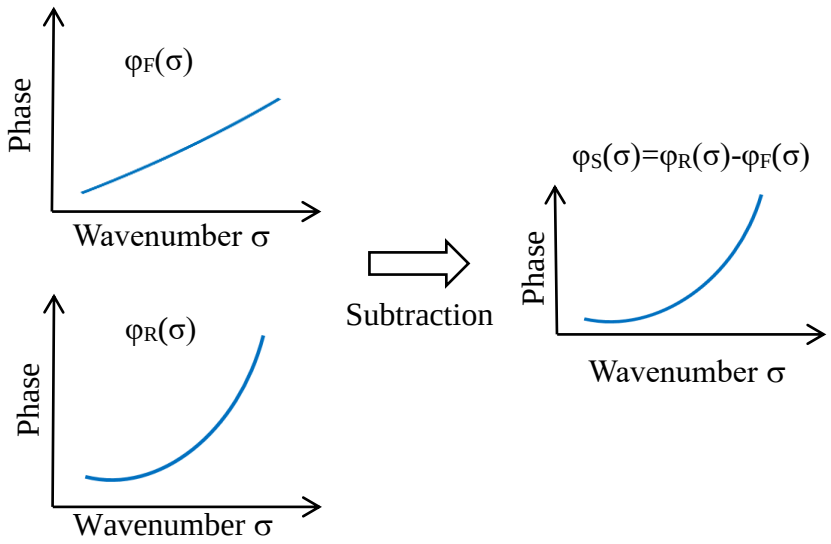

Fig. 1.13. Elimination of dispersion effect generated by BS.

1.2.1.4. Different optical configurations

Since the spectral phase $\varphi_S(\sigma)$ is expressed as $\varphi_S(\sigma)=4\pi n(\sigma)T\sigma$, it is required that $n(\sigma)$ is eliminated from $\varphi_S(\sigma)$ for the thickness measurement. This

elimination is achieved by constructing two optical configurations shown in Fig. 1.14. Another reference surface is put behind the object, and interference signal $S_{R1}(\sigma)$ is generated by the two beams reflected from the two reference surfaces in the configuration of (a). Interference signal $S_{R2}(\sigma)$ is generated by the two beams without the object in the configuration of (b).The spectral phases obtained from the $S_{R1}(\sigma)$ and $S_{R2}(\sigma)$ are expressed as $\varphi_{R1}(\sigma)$ and $\varphi_{R2}(\sigma)$. Term of $[n(\sigma)\text{-}1]T$ exists in spectral phase $\varphi_{SR}(\sigma)=\varphi_{R1}(\sigma)\text{-}\varphi_{R2}(\sigma)$. Hence the term of $n(\sigma)T$ is eliminated by $\varphi_S(\sigma)\text{-}\varphi_{SR}(\sigma)$. Thickness T is measured from the spectral phase $\varphi_S(\sigma)\text{-}\varphi_{SR}(\sigma)=T$. Therefore, different optical configurations are constructed to get a value of T from the different spectral phases. In this case the values of $n(\sigma)$ are not required for the thickness measurement. Large thickness T less than 2 mm can be measured by the methods described above where variable reference position, low-resolution SPA, and different spectral phases in different optical configurations are used.

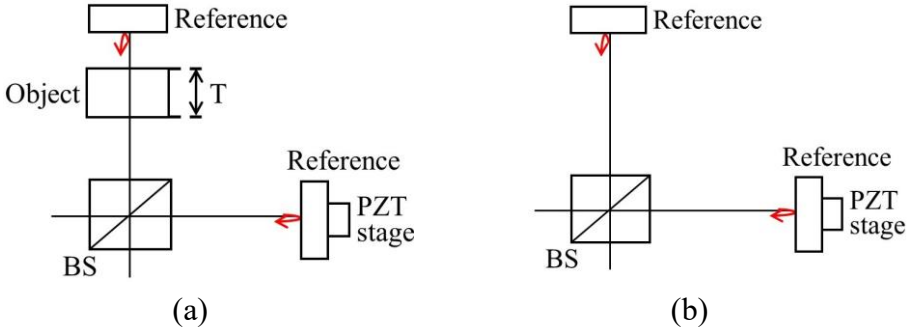

Fig. 1.14. Optical configurations to generate interference signals (a) $S_{R1}(\sigma)$ and (b) $S_{R2}(\sigma)$.

1.2.1.5. Measurement of more large thickness

In order to measure more large T value, a compensation glass (CG) is used to reduce the dispersion effect due to the object. Refractive index of the CG is known and is the same as that of the object. Thickness of the CG is T_C which is almost equal to T. Spectral phase $\varphi(\sigma)$ containing terms of $n(\sigma)(T\text{-}T_C)$ and T is obtained from different spectral phases detected in different optical configurations, and the distribution of $\varphi(\sigma)$ consists of nonlinear and linear components [C1.7] as shown in Fig. 1.15. Nonlinear component of $\varphi(\sigma)$ is produced by the term of $n(\sigma)(T\text{-}T_C)$, and it is utilized to estimate a value of $T\text{-}T_C$ through comparing the two distributions of the detected nonlinear component and the theoretical nonlinear component using the known refractive index $n(\sigma)$. The value of T is obtained from the detected $\varphi(\sigma)$ by using the estimated value of $T\text{-}T_C$. Thus, large thickness T more than 2 mm can be measured by this method using the CG and the nonlinear component of spectral phase.

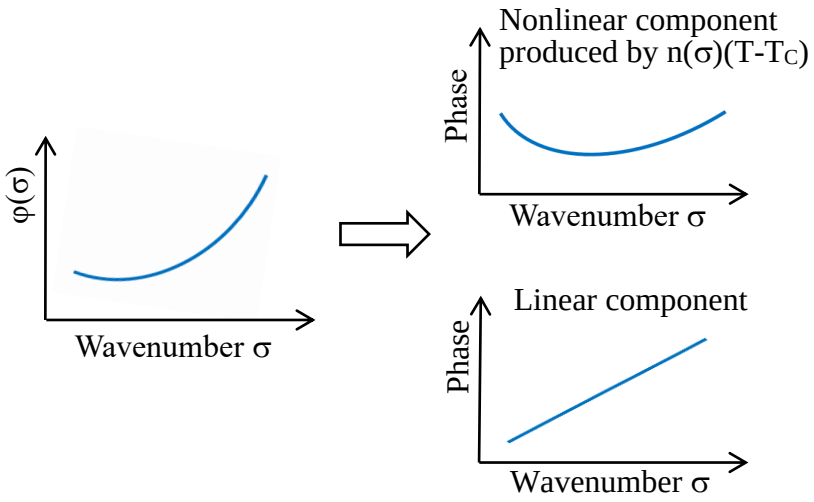

Fig. 1.15. Nonlinear and linear components of spectral phase $\varphi(\sigma)$.

1.2.2. Refractive index measurement

Important property of optical material is phase refractive index $n(\sigma)$. Figure 1.16 shows an example about effect of $n(\sigma)$, where a beam from a light source has a broad spectrum $I(\sigma)$. When this beam passes through a glass plate with thickness T, the optical path length is increased by $n(\sigma)T$. Since the optical path length at each wavenumber is not identical to each other, the input beam with a sharp pulse along time axis is changed to a distorted beam by the effect of refractive index $n(\sigma)$. Therefore the measurement of refractive index is important.

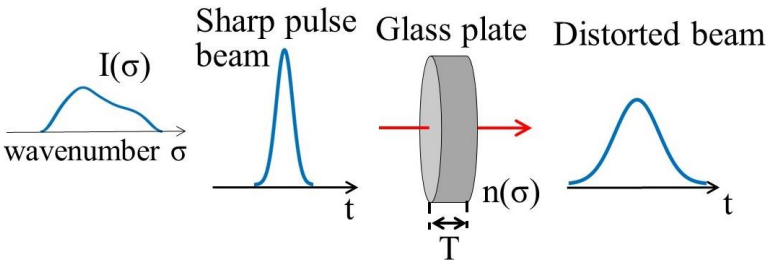

Fig. 1.16. Effect of refractive index $n(\sigma)$ on sharp pulse beam.

Spectrally resolved interferometers (SRIs) are more useful than white light scanning interferometers for measurement of phase refractive index $n(\sigma)$ because the interference signal of SRI is detected in the wavenumber domain. Figure 1.17 shows a schematic configuration of SRI for measuring refractive index, where object is a glass plate. An input beam comes from a white light source. Interference signal $S(\sigma)=I(\sigma)\cos[4\pi n(\sigma)T\sigma]$ is generated by the two

beams reflected from the front surface and rear surface of the glass plate, where π rad contained in the beam reflected from the front surface of glass plate is ignored for the sake of simplicity. Spectral phase $\varphi(\sigma)=4\pi n(\sigma)T\sigma$ is obtained from $S(\sigma)$ as described in Sec.1.1.3. This $\varphi(\sigma)$ is a theoretical distribution, and it is denoted as $\varphi_T(\sigma)=4\pi n(\sigma)T\sigma$. When the measurement of T is made with the method described in Sec.1.2.1, the refractive index of $n(\sigma)=\varphi_T(\sigma)/4\pi T\sigma$ can be obtained by using a measured value of T.

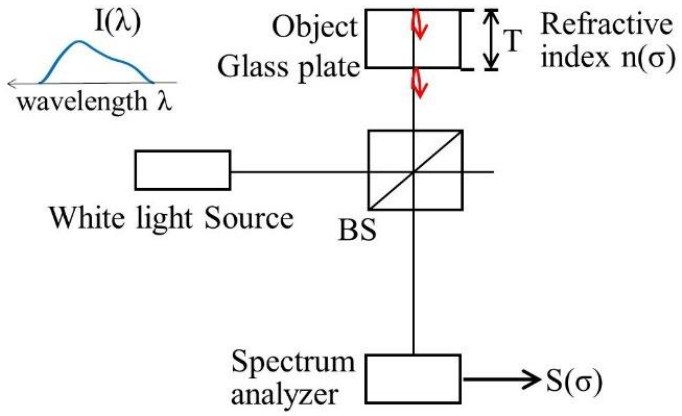

Fig. 1.17. Schematic configuration of SRI.

However, a spectral phase calculated from the detected interference signal through performing Fourier transform and inverse Fourier transform is wrapped in the region from -π to π. Since this calculated phase is unwrapped to get an unwrapped phase $\varphi_M(\sigma)$, phase ambiguity 2π exists in $\varphi_M(\sigma)$. Thus, it is required to determine 2π phase ambiguity existing in the unwrapped phase $\varphi_M(\sigma)$ to get the $n(\sigma)$.

Conventional methods to determine 2π phase ambiguity have been reported, but a new method is needed as described below. One conventional method is to measure a phase refractive index at one wavenumber with another instrument [C1.8]. Another instrument makes a measurement setup complicated. Another conventional method is to use group refractive index $n_G(\sigma)$ which is calculated by differentiating the unwrapped phase $\varphi_M(\sigma)$ [C1.9]. By the differentiation a constant value $2\pi p$ of phase ambiguity disappears in $n_G(\sigma)$, where p is an integer. In order to obtain $n(\sigma)$ from a group index detected from a spectral phase, $n(\sigma)$ is expressed by an equation having some coefficients and an equation of $n_G(\sigma)$ is derived with the relation of $n_G(\sigma)=n(\sigma)+\sigma[dn(\sigma)/\sigma]$. A detected group index is fitted with the equation of the group index to determine the coefficients in the equation of $n(\sigma)$. Since the measured refractive index is expressed by the equation with the determined coefficients, it is not exactly equal to an actual phase refractive index. Therefore, a new method is required to get an actual refractive index from the unwrapped phase $\varphi_M(\sigma)$ detected with a SRI.

Phase distributions are shown schematically by using straight lines in Fig. 1.18. The theoretical phase of $\varphi_T(\sigma)=4\pi n(\sigma)T\sigma$ is represented by blue line. The phase calculated from the interference signal is represented from σ_S by dark line. This calculated phase is unwrapped from σ_S as represented by red line. Since the unwrapped phase contains phase ambiguity of $2\pi p$, it can be expressed mathematically by $\varphi_M(\sigma)=4\pi n(\sigma)T\sigma-2\pi p$ in the region from $\sigma=0$. Actually the calculated phase and $\varphi_M(\sigma)$ are not detected in the region from $\sigma=0$ to $\sigma=\sigma_S$, which is represented by the dotted lines. The red dotted line has a value of $-2\pi p$ at $\sigma=0$ because of $\varphi_M(\sigma)=4\pi n(\sigma)T\sigma-2\pi p$. In Fig. 1.18, p is equal to 2. The unwrapped phase $\varphi_M(\sigma)$ is fitted with a fitting function $f(\sigma)$ which is expressed as, for example, $f(\sigma)=4\pi T(b_0+b_2\sigma^2)\sigma-2\pi p_f$. The green line in Fig. 1.18 is the distribution of $f(\sigma)$ with the fitted values of b_0 and b_2, and it is generally different from the distribution of $\varphi_M(\sigma)$. The value of p_f is obtained from $f(0)=-2\pi p_f$. If the fitted distribution of $f(\sigma)$ is the same as that of $\varphi_M(\sigma)$, the result of $p_f=p$ is obtained. But generally the fitted $f(\sigma)$ is different from $\varphi_M(\sigma)$ as shown in Fig. 1.18. When the absolute value of p_f-p is smaller than 0.5, the value of p can be obtained by rounding off the value of p_f. Therefore, an actual refractive index of $n(\sigma)=[\varphi_M(\sigma)+2\pi p]/4\pi T\sigma$ is achieved from the detected spectral phase distribution after determining the phase ambiguity $2\pi p$. Refractive index measurement by this method is described in chapter 4.

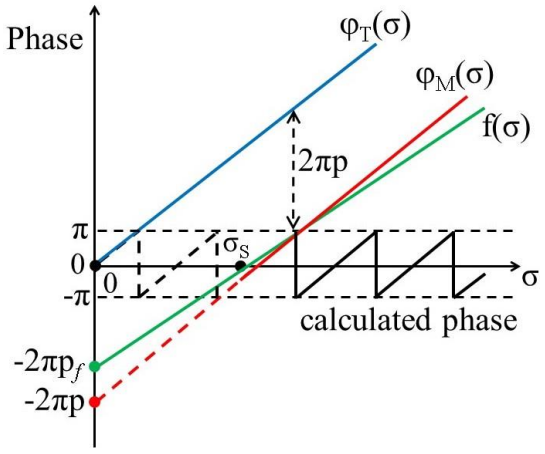

Fig. 1.18. Schematic representations of $\varphi_T(\sigma)$, calculated phase, $\varphi_M(\sigma)$, and $f(\sigma)$.

1.3. Organization of the thesis

Sec. 1.1 describes three different interferometers to explain why this thesis adopts a spectrally resolved interferometer, as shown in Fig. 1.19. Section 1.1.1 describes single wavelength interferometer. The measurable range of this interferometer is limited. In order to eliminate this limitation, white light scanning interferometer (WLSI) is described in Sec. 1.1.2. However, WLSI requires exact scanning positions to achieve an exact measurement. As a

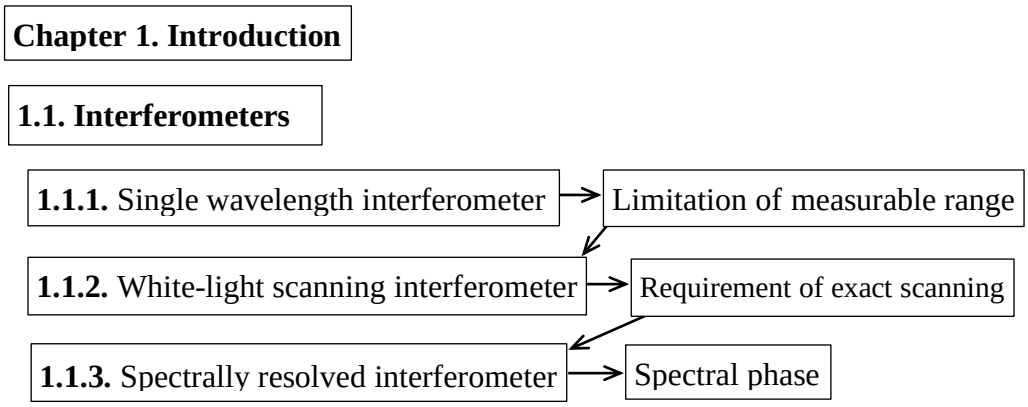

Fig. 1.19. “1.1. Interferometers”.

better interferometer, spectrally resolved interferometer (SRI) is described in Sec. 1.1.3, where the interference signal $S(\sigma)$ is detected along wavenumber σ with using a spectrum analyzer. Phase term contained in the $S(\sigma)$ is extracted and it is called spectral phase. Thus spectral phase is utilized in this thesis for measurements.

In Sec. 1.2 motivations for measurements of thickness and refractive index are explained. Thickness measurement is described in Sec. 1.2.1 which has five subsections. Subsections from Sec.1.2.1.1 to 1.2.1.4 lead to Chapter 2, as shown in Fig. 1.20. These subsections are explained as below.

Sec.1.2.1.1 : In order to measure a large thickness T of glass plate, a high resolution SPA is required because the period of the $S(\sigma)$ is small. Thus variable position of the reference surface is proposed where the reference position is adjusted so that a large period is generated in the $S(\sigma)$. This $S_R(\sigma)$ can be detected with low resolution SPA.

Sec.1.2.1.2 : Amplitude distribution $|F_R(d)|$ of Fourier transform of interference signal has a wide spread because of the dispersion effect of $n(\sigma)T$. Hence the peak position of amplitude distribution does not have a clear relation with the OPD. On the other hand, the dispersion effect of $n(\sigma)T$ produces non-linear distribution for spectral phase. But since the spectral phase is directly related with OPD, the spectral phase can be used to extract useful information such as thickness T and refractive index $n(\sigma)$ about object.

Sec.1.2.1.3 : The different length in the two sides of the BS produces dispersion effect due to $n_B(\sigma)l_\varepsilon$. Two different spectral phases calculated from interference signals generated through the BS contain the term of $n_B(\sigma)l_\varepsilon$. The dispersion effect of $n_B(\sigma)l_\varepsilon$ is eliminated by the subtraction between the two calculated phases.

Sec.1.2.1.4 : Spectral phases in different optical configurations contain the terms of $n(\sigma)T$ and $[n(\sigma)\text{-}1]T$. In order to calculate T, it is required to eliminate the terms of $n(\sigma)T$. This elimination is achieved by performing subtractions in the spectral phases. In this case the values of $n(\sigma)$ are not required for the thickness measurement. Therefore, in chapter 2 large thickness

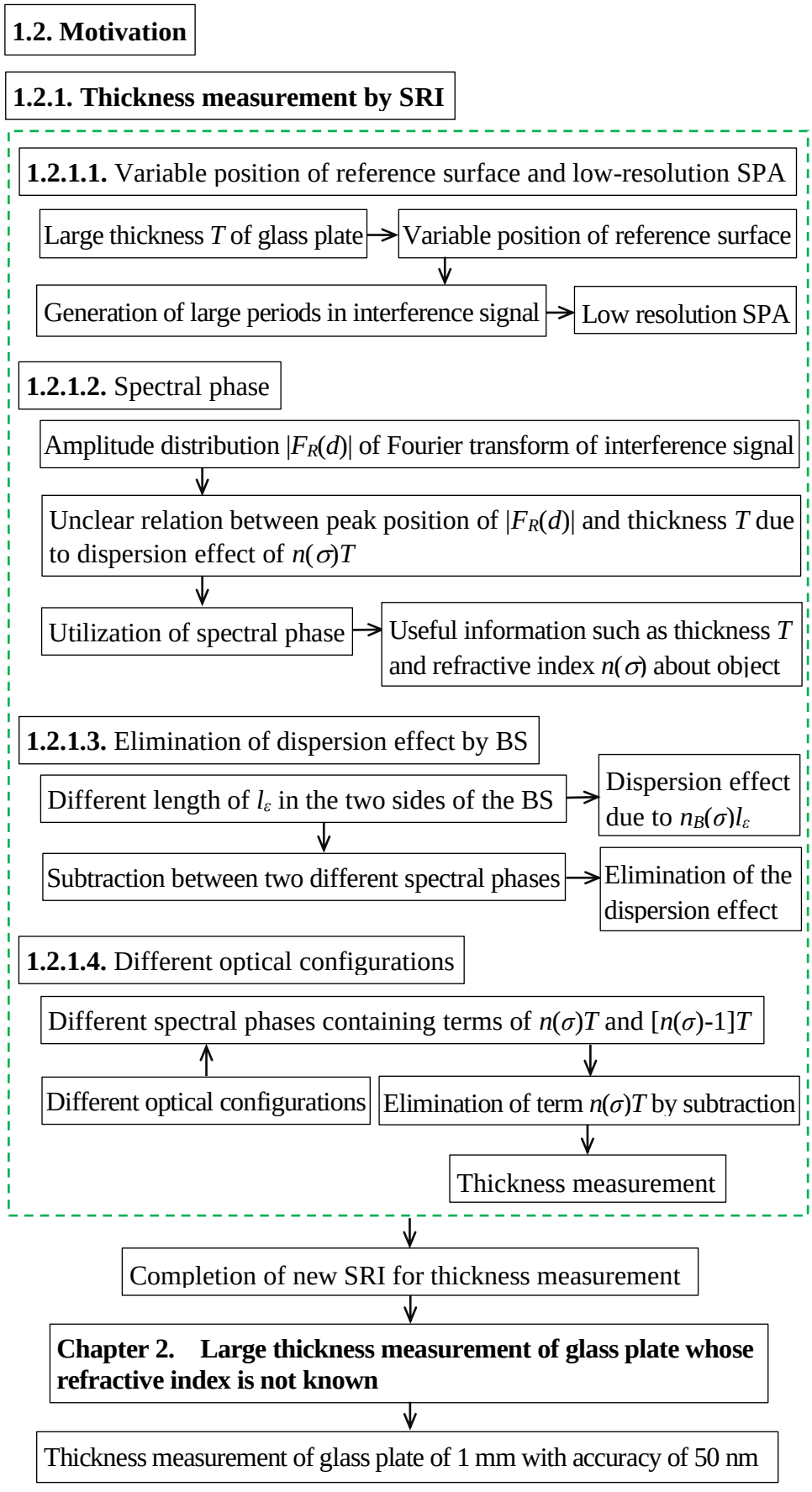

Fig. 1.20. “1.2.1. Thickness measurement by SRI” leading to Chapter 2.

less than 2 mm can be measured by using variable reference position, low-resolution SPA, and different spectral phases in different optical configurations.

It is required to reduce the dispersion effect caused by $n(\sigma)T$ for more larger thickness measurement. This reduction is achieved by using a compensation glass CG of thickness T_C. Section 1.2.1.5 explains this measurement which leads to Chapter 3, as shown in Fig. 1.21. Spectral phase $\varphi(\sigma)$ containing the terms of $n(\sigma)(T\text{-}T_C)$ and T is obtained from different spectral phases detected in different optical configurations. The detected nonlinear component of $\varphi(\sigma)$ and the theoretical nonlinear component with known refractive index are compared to estimate the value of $T\text{-}T_C$. Finally the value of T is obtained from $\varphi(\sigma)$ by using the estimated value of $T\text{-}T_C$. In chapter 3, thickness of glass plate of 5 mm can be measured with accuracy of 2 μm.

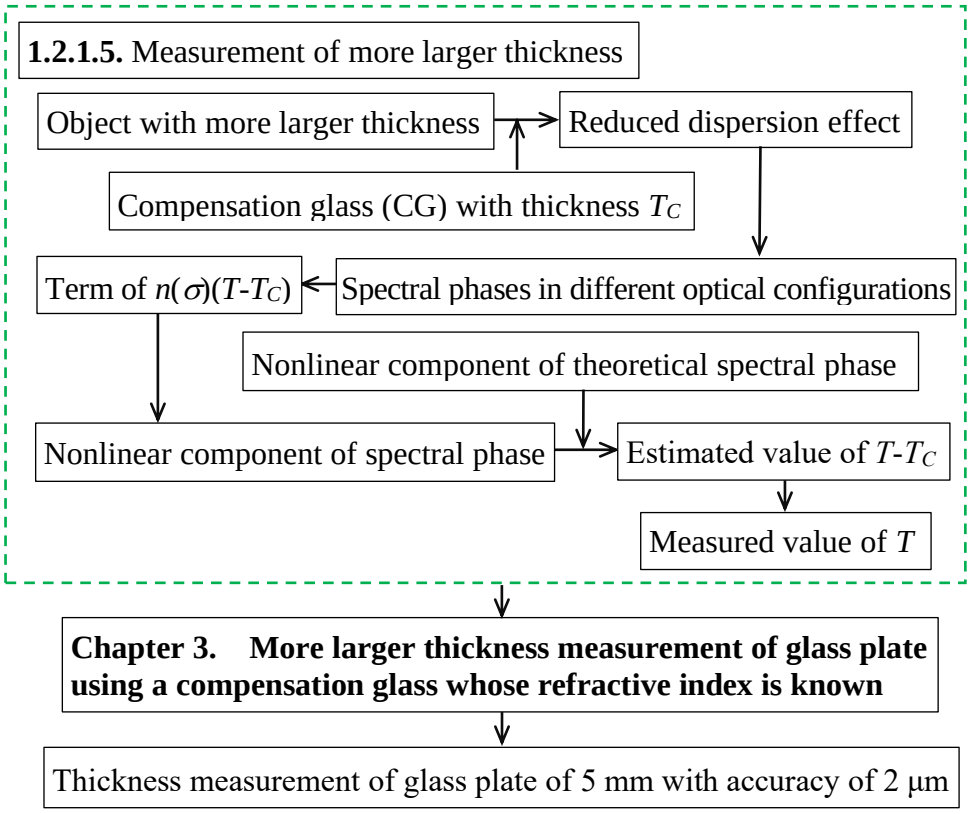

Fig. 1.21. "1.2.1.5. Measurement of more larger thickness" leading to Chapter 3.

Measurement of refractive index $n(\sigma)$ from a spectral phase is described in Sec. 1.2.2, as shown in Fig. 1.22. Section 1.2.2 leads to Chapter 4. Since the calculated spectral phase $\varphi_M(\sigma)$ is unwrapped from σ_S, $\varphi_M(\sigma)$ has phase ambiguity $2\pi p$ compared to the theoretical spectral phase $\varphi_T(\sigma)$. This phase ambiguity is estimated by fitting $\varphi_M(\sigma)$ with a fitting function $f(\sigma)$, where a

measured value of thickness T is used in $f(\sigma)$. If the absolute value of difference between p and the fitted value of p_f=$f(0)$ is less than 0.5, p can be obtained by rounding off p_f. Therefore, measurement of an actual refractive index of $n(\sigma)$ is achieved from the detected spectral phase distribution after determining the phase ambiguity $2\pi p$.

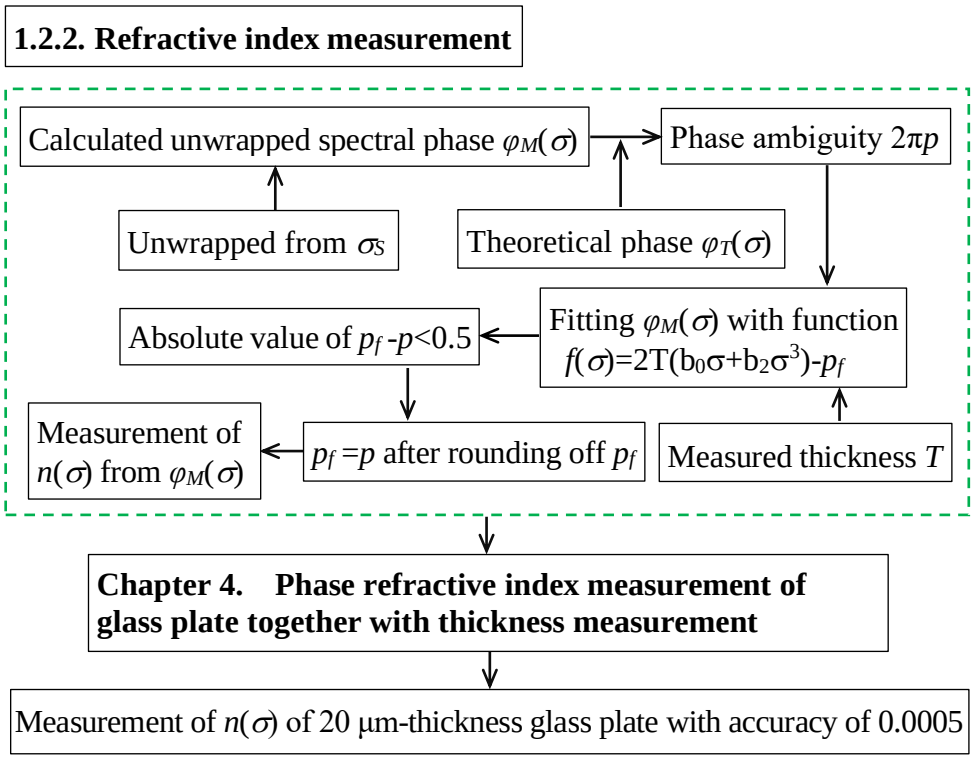

Fig. 1.22. “1.2.2. Refractive index measurement” leading to Chapter 4.

Finally, in Chapter 5 the conclusions are summarized to explain that the measurements of large thickness and refractive index are achieved with the unique SRI and the spectral phases. Large thickness of a glass plate less than 2 mm can be measured by using variable reference position as described in chapter 2. In chapter 3, the dispersion effect due to a large thickness T more than 2 mm is reduced by using a CG. The value of T is obtained through using the nonlinear component of spectral phase. Refractive index measurement is achieved in chapter 4, where $n(\sigma)$ is obtained from the detected spectral phase distribution after determining the phase ambiguity $2\pi p$.

CHAPTER 2

LARGE THICKNESS MEASUREMENT OF GLASS PLATE WHOSE REFRACTIVE INDEX IS NOT KNOWN

2.1. Introduction

Interferometer have been widely used for thickness measurement with rapid progress of precision manufacturing industry. Interferometer have been widely used for thickness measurement with rapid progress of precision manufacturing industry. Measurements of thin-film thickness with spectrally resolved interferometers (SRIs) have been reported in many papers [C2.1-C2.7]. In SRIs many wavelengths contained in the light source are separated with a diffraction grating to get an interference signal distributed along wavelength. Since the interference signal is detected with a line sensor in a spectral analyzer, the maximum measurable thickness is limited by the resolution of the spectral analyzer. When a spectral analyzer with a high resolution of 0.06 nm was used, the thickness of a few millimeters was measured with measurement error of about a few hundred nanometers with the light source whose central wavelength and bandwidth were about 1300 nm and 40 nm, respectively [C2.1, C2.2]. Recently a portable and inexpensive spectral analyzer is widely employed to construct a SRI easily, but the resolution of the spectral analyzer is not so high. Hence a technique for extending the maximum measurable thickness in a SRI with a low resolution spectral analyzer must be proposed by analyzing the amplitude distribution of Fourier transform of the interference signal. Moreover, in many papers [C2.1-C2.4, C2.6, C2.7] optical path differences contained in an interference signal are extracted from peak positions in the amplitude distribution of Fourier transform of the interference signal. However the peak position does not exactly correspond to an optical path difference which contains a path in a dispersion medium. On the other hand a slope of spectral phase distribution of an interference signal along wavenumber provides a more exact optical path difference than the peak position. And a large bandwidth of a light source is better to get a small measurement error in calculating the slope of spectral phase distribution. In order to measure exactly a large thickness of glass plate with a SRI using a spectral analyzer with a low resolution of 0.5 nm and a supercontinuum light source with a large bandwidth of about 300 nm, a new measurement method with the SRI is proposed where the measurement range is extended by moving a reference surface with a piezoelectric transducer (PZT) stage. First, Fourier transform of an interference signal produced by a rear surface of glass plate is analyzed in details to make it clear how to extend

the measurement range. This Fourier transformed signal has a large spread width in the amplitude distribution caused by dispersion effect of the glass plate. The central position of the spread width is called signal position. It is made clear that the amplitude distribution is not symmetric about the signal position. The signal position is adjusted by the position of the reference surface so that the interference signal can be detected with the low resolution spectral analyzer. The measurable maximum thickness is derived by considering the resolution of the spectral analyzer and the dispersion effect of the glass plate. Next, the measurement method is presented where four different optical configurations are used together with four different signal positions. Through this four-step measurement the thickness of the glass plate can be obtained from a slope of a spectral phase distribution which does not contain the refractive index of glass plate. Finally, in experiments the positions of the glass plate and an additional reference surface are calculated roughly from the signal positions, and a dispersion effect of the beam splitter are made clear from a spread width. And then it is confirmed that the detected values of the signal positions agree with the theoretical values. A small measurement error of 50 nm is achieved in measuring 1 mm thickness of a glass plate.

2.2. Principle

2.2.1. Interference signal with a variable signal position

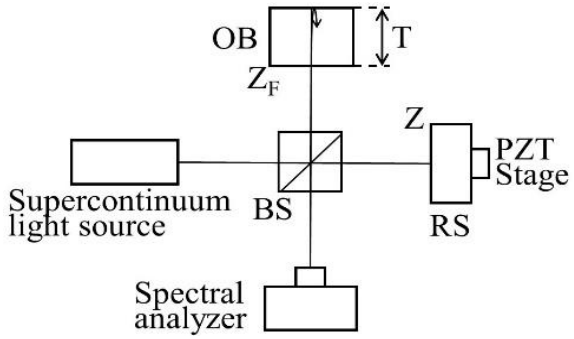

Fig. 2.1. Schematic configuration of SRI for measuring thickness of a glass plate.

Schematic configuration of a SRI is shown in Fig. 2.1. An interference signal generated by a rear surface of an object (OB) is analyzed to make it clear how a variable signal position is working well in a SRI with a low resolution spectral analyzer. The variable signal position is provided by changing a position *Z* of a reference surface (RS) with a piezoelectric transducer (PZT) stage. A beam from supercontinuum light source is divided by a beam splitter

(BS) for the object and reference arms, and the two beams from the two arms are combined again by the BS to generate an interference signal. Spectral intensity $I(\sigma)$ of the supercontinuum light source is shown in Fig. 2.2, where σ is wavenumber and the spectral range is about from 500 to 800 nm with a central wavelength of 650 nm. The OB is a glass plate of BK7 with thickness T and refractive index $n(\sigma)$. The interference signal is detected by a spectral analyzer whose resolution $\Delta\lambda$ is 0.5 nm. When the position of front surface of the OB is Z_F and the position of the RS is Z, the interference signal $S(\sigma)$ is expressed as

$$S(\sigma) = I(\sigma) + I(\sigma)\cos\{4\pi[Z_F + n(\sigma)T - Z]\sigma\}, \tag{2.1}$$

where the phase π arisen in the reflection by the rear surface of the OB is ignored for the sake of simplicity. An interference signal $S(\lambda)$ detected with a constant interval of $\Delta\lambda$=0.5 nm is converted to $S(\sigma)$ with a constant interval of $\Delta\sigma_A$ by an interpolation formula. Interval $\Delta\sigma$ corresponding to two wavelengths of λ and $\lambda+\Delta\lambda$ is given by

$$\Delta\sigma = (1/\lambda) - [1/(\lambda + \Delta\lambda)] \cong \Delta\lambda / \lambda^2. \tag{2.2}$$

By using the weighted average wavelength λ_A of the spectral intensity as λ in Eq. (2.2), the constant interval of $\Delta\sigma_A=\Delta\lambda/\lambda_A^2$ is decided for the interpolation. A least square line of $a_0+a_1\sigma$ is defined for the distribution of $n(\sigma)\sigma$, and it is considered that $n(\sigma)T\sigma=a_1T\sigma+(n(\sigma)-a_1)\sigma T$ in Eq. (2.1). Then Fourier transform of $S(\sigma)$ or Fourier transformed signal which is a function of distance d is given by

$$F(d) = F_I(d) + F_I\left(d - 2(Z_F + a_1T - Z)\right) \otimes \Im\{(1/2)\exp[\, j4\pi\{n(\sigma)\sigma - a_1\sigma\}T\,]\}$$

$$+F_I\left(d + 2(Z_F + a_1T - Z)\right) \otimes \Im\{(1/2)\exp[-j\{n(\sigma)\sigma - a_1\sigma\}T\,]\}, \tag{2.3}$$

where $\Im$ and $\otimes$ mean Fourier transform and convolution, respectively, and $F_I(d)= \Im\{I(\sigma)\}$. From Eq. (2.3) a variable signal position is given by

$$d_S = 2(Z_F + a_1T - Z). \tag{2.4}$$

The variable signal position is equal to the difference between the optical path of Z_F+a_1T in the object arm and that of Z in the reference arm. Equation (2.3) is rewritten as

$$F(d) = F_I(d) + F_I(d - d_S) \otimes F_T(d) + F_I(d + d_S) \otimes F_T^*(-d) = F_I(d) + F_S(d) + F_S^*(-d), \tag{2.5}$$

Where $F_T(d)=\Im\{(1/2)\exp[j4\pi\{n(\sigma)-a_1\}T\sigma]\}$ and * mean complex conjugate. Figure 2.3 shows the amplitude distribution of $F(d)$ obtained by simulations, where T=997.4 μm, Z_F-Z=-1587 μm, and $\Delta\sigma_A=0.5\times10^{-3}/0.6^2=1.3\times10^{-3}$ μm^{-1}. Although the maximum detectable distance d_{max} in $F(d)$ is $1/(2\Delta\sigma_A)$=385 μm, the maximum distance for $F_S(d)$ is limited to $d_L=d_{max}/2$=193 μm to distinguish the components of $F_S(d)$ from noise components at larger distances. The

amplitude distribution of $F(d)$ in region of $d \geq 0$ is used for the measurement. In the simulations the Sellmeier equation of BK7 glass is used as the refractive index $n(\sigma)$, and a_1=1.540 is obtained from calculating a least square line in the region from σ_S=1.2 μm^{-1} to σ_E=2.1 μm^{-1}. In Fig. 2.3, d_S=-102 μm from Eq. (2.4), and the spread width W_I of $F_I(d)$ and W_S of $F_S^*(-d)$ are 12 μm and 68 μm, respectively. Simulation results at different values of thickness T μm make it clear that the W_S=12+0.056T μm holds with error less than 0.4 μm in the region of T from 500 μm to 2200 μm. From Eq. (2.5) and the simulation results shown in Fig. 2.3 it is concluded that the spread width W_S is caused by both W_I and dispersion effect of $n(\sigma)$, and also that the position of d_S is the center of width W_S.

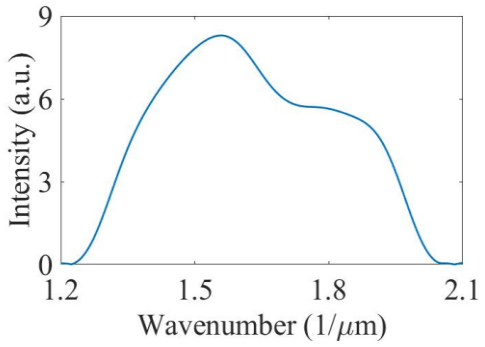

Fig. 2.2. Spectral intensity I(σ) of supercontinuum light source used in experiments.

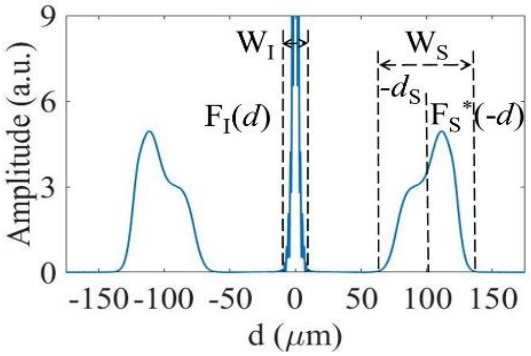

Fig 2.3. Amplitude distributions of F(d) when d_S is a minus value.

An interference signal $S(\sigma)$ detected in experiments is shown in Fig. 2.4, and its amplitude distribution $F(d)$ is shown in Fig. 2.5, where the conditions of T, Z_F-Z, and $\Delta\sigma_A$ are the same as those in Fig. 2.3. The spread width W_I and W_S are 12 μm and about 67 μm, respectively, and d_S=-102 μm. The values of W_I, W_S, and d_S are almost equal to those in Fig. 2.3, but many signal components exist in the width of W_N=62 μm. It is seemed that the signal components in the region of W_N were caused by mechanical vibrations of the

interferometer and electronics noise of the spectral analyzer. Components of $F_S^*(-d)$ exist in the region of distance larger than $W_I/2+W_N$=68 μm. Since the d_S locates at the center of width W_S, the position Z of RS is determined so that $|d_S|=|2(Z_F+a_1T-Z)|$ is larger than $W_I/2+W_N+W_S/2$=68+(12+0.056T)/2 μm. The relation of $W_I/2+W_N+W_S=d_L$ decides the maximum measureable thickness T_m. The solution of 68+(12+0.056T)=193 μm leads to T_m=2018 μm.

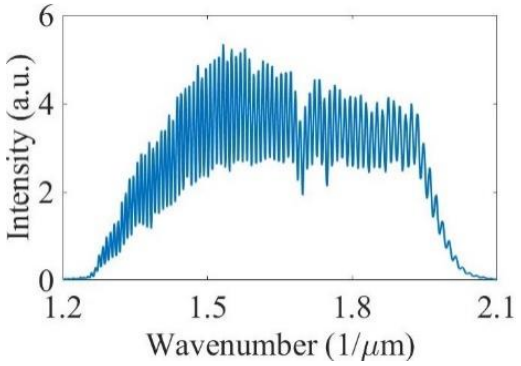

Fig. 2.4. Detected interference signal $S(\sigma)$.

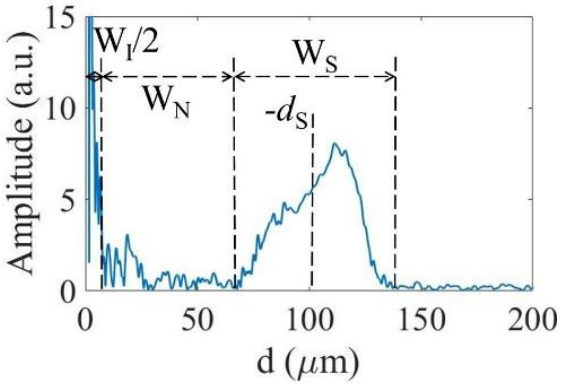

Fig. 2.5. Amplitude distribution of $F(d)$ at d_S<0.

2.2.2. Principle of thickness measurement

Figure 2.6 shows the configuration of a SRI with a low resolution spectral analyzer. An OB and a fixed reference surface 2 (RS2) are contained in the object arm, and the reference arm contains a reference surface 1 (RS1) fixed on a PZT stage. The RS1 is moved by the PZT stage to a specified position to produce an interference signal which can be detected with the low resolution spectral analyzer. Four-step measurement is carried out to make thickness measurement as shown in Fig. 2.7. In step 1, the RS1 is moved to a position of Z_1 and the optical path difference (OPD) is equal to Z_F-$n_B(\sigma)l_\varepsilon$-Z_1, where Z_F is the position of the front surface of OB, l_ε is the difference between the two paths of the object and reference beams propagating in the BS, and $n_B(\sigma)$

is the refractive index of BS. This l_ε is caused by the different lengths of the two sides in the BS. The interference signal except the first term of $I(\sigma)$ in Eq. (2.1) is expressed as

$$S_1(\sigma) = I(\sigma)\cos\{4\pi[Z_F - n_B(\sigma)l_\varepsilon - Z_1]\sigma\}. \quad (2.6)$$

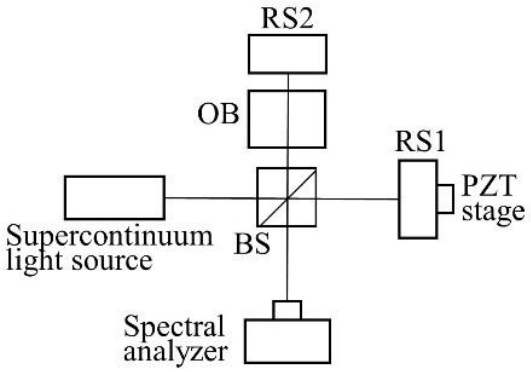

Fig. 2.6. Schematic configuration of spectral resolved interferometer using variable difference frequency.

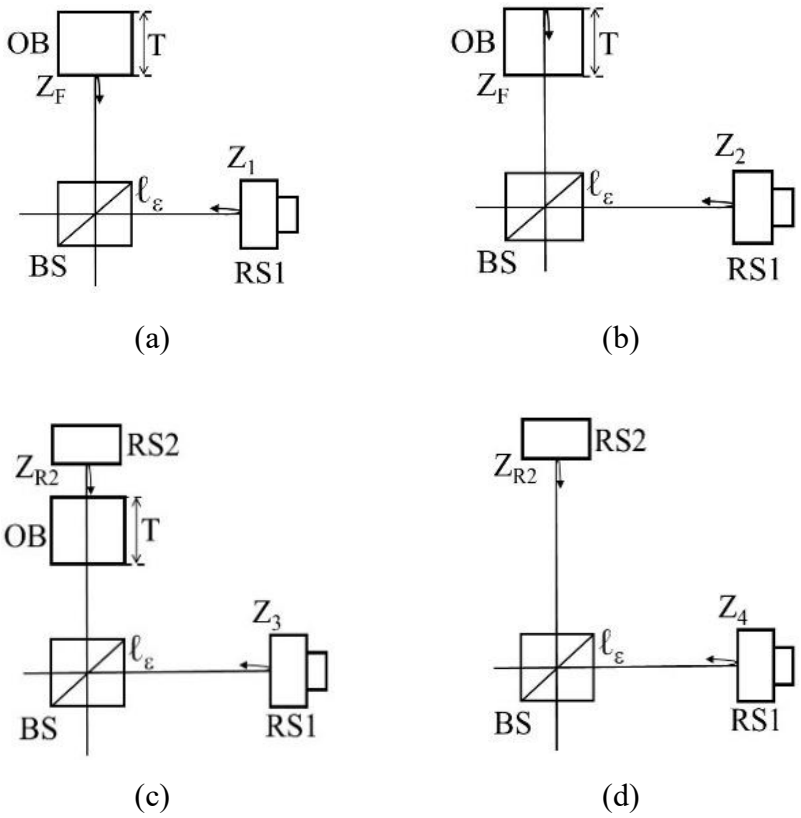

Fig. 2.7. Configuration of four-step measurements.

Signal processing is carried out in the same way as described in Sec. 2.2.1. And all of the notations defined in Sec. 2.2.1 have suffix of *i* that means step

i hereafter. A rectangular window having the width slightly larger than the spread width W_{S1} of $F_{1S}^{*}(-d)$ is used to select $F_{1S}^{*}(-d)$ from $F_1(d)$ at $d_{S1}<0$. Inverse Fourier transform is performed on this windowed distribution to get the following distribution:

$$S_{1F}(\sigma) = I(\sigma)\exp\{-\mathrm{j}4\pi[Z_F - n_B(\sigma)l_\varepsilon - Z_1]\sigma\}. \tag{2.7}$$

The unwrapped phase of $S_{1F}(\sigma)$ is extracted as

$$\varphi_1(\sigma) = -4\pi[Z_F - n_B(\sigma)l_\varepsilon - Z_1]\sigma. \tag{2.8}$$

In step 2, the RS1 is moved by the PZT stage to a new position of Z_2 for reducing the OPD between the two beams reflected from the rear surface of OB and the RS1, and the interference signal is expressed as

$$S_2(\sigma) = I(\sigma)\cos\{4\pi[Z_F + n(\sigma)T - n_B(\sigma)l_\varepsilon - Z_2]\sigma - \pi\}, \tag{2.9}$$

where π arises due to the beam reflected by the rear surface of OB. By the same signal processing as in step 1, the unwrapped phase is given by

$$\varphi_2(\sigma) = -4\pi[Z_F + n(\sigma)T - n_B(\sigma)l_\varepsilon - Z_2]\sigma + \pi, \tag{2.10}$$

By combining $\varphi_1(\sigma)$ and $\varphi_2(\sigma)$ to eliminate $n_B(\sigma)l_\varepsilon$, a measurement value of D_1 is obtained as

$$D_1(\sigma) = \varphi_2(\sigma) - \varphi_1(\sigma) = 4\pi(Z_2 - Z_1 - n(\sigma)T)\sigma + \pi. \tag{2.11}$$

In step 3, the RS1 is moved to a position of Z_3 for reducing the OPD between the two beams reflected from the RS1 and the RS2. The unwrapped phase of interference signal $S_3(\sigma)$ is given by

$$\varphi_3(\sigma) = -4\pi[Z_{R2} + (n(\sigma) - 1)T - n_B(\sigma)l_\varepsilon - Z_3]\sigma. \tag{2.12}$$

In step 4, the OB is removed from the object arm and the RS1 is moved to a position of Z_4 for compensating the OPD change arisen by the removal of OB. The unwrapped phase of interference signal $S_4(\sigma)$ is given by

$$\varphi_4(\sigma) = -4\pi[Z_{R2} - n_B(\sigma)l_\varepsilon - Z_4]\sigma. \tag{2.13}$$

By eliminating Z_{R2}-$n_B(\sigma)l_\varepsilon$ with Eqs. (2.12) and (2.13), a measurement value of $D_2(\sigma)$ is expressed as

$$D_2(\sigma) = \varphi_4(\sigma) - \varphi_3(\sigma) = 4\pi[Z_4 - Z_3 + (n(\sigma) - 1)T]\sigma. \tag{2.14}$$

A measurement value of $D_3(\sigma)$ is obtained from $D_1(\sigma)$ and $D_2(\sigma)$ as follows:

$$D_3(\sigma) = -D_1(\sigma) - D_2(\sigma) = 4\pi[Z_1 - Z_2 + Z_3 - Z_4 + T]\sigma - \pi. \tag{2.15}$$

Finally, by denoting the slope of a least square line in the distribution of $D_3(\sigma)$ as $slope[D_3(\sigma)]$, the thickness of T can be obtained as

$$T = slope[D_3(\sigma)]/4\pi - (Z_1 - Z_2 + Z_3 - Z_4). \tag{2.16}$$

2.3. Experimental results

The SRI was constructed as shown in Fig. 2.6 for single point thickness measurement of a glass plate. The RS1 and the RS2 were one reflecting surface of a glass plate with wedged angle. The RS1 was fixed on a PZT stage with 0.5 nm resolution and 10 nm repeatability of positioning. Both the BS and the OB were BK7 glass and the thickness of OB was about 1mm. The interference signal was detected with a spectral analyzer with 0.5 nm resolution. Since the interfering optical fields were fed into the spectral analyzer by an optical fiber with a 250 μm core diameter, the spatial resolution of the SRI was 250 μm. The signal processing carried out in step 1 to step 4 was the method described in Secs. 2.2.1 and 2.2.2 whose contents correspond to step 2. The reference position Z_i in step i was determined so that variable signal position d_{Si} is larger than $W_I/2+W_{Ni}+W_{Si}/2$.

In step 1, the PZT stage was moved and stopped at position Z_1=0.000 μm as an origin for other reference positions. The interference signal $S_1(\sigma)$ detected in the region from σ_S =1.2 μm^{-1} to σ_E =2.1 μm^{-1} is shown in Fig. 2.8 (a). Figure 2.8 (b) shows the amplitude distribution of $F_1(d)$ in the region of d>0. W_{S1} and W_{N1} were about 13 μm and 19 μm, respectively. Since this W_{S1} was caused by $n_B(\sigma)l_\varepsilon$ as shown by Eq. (2.6), l_ε was calculated to be about 20 μm from the relation of W_{S1}=13=12+0.056l_ε μm with error of about 1 μm. Since the amplitude of $F_1(d)$ was larger than that of $F_2(d)$ shown in Fig. 2.5, W_{N1} was smaller than W_{N2}=62 μm. The signal position was -d_{S1}=62 μm which was larger than $W_I/2+W_{N1}+W_{S1}/2$=6+19+(13/2)=32 μm. From d_{S1}=2(Z_F-a_1l_ε-Z_1)=2(Z_F-1.54×20-0)=-62 μm, Z_F=0 was obtained. A rectangle window existing from d=54 μm to d=69 μm was used to select the component of F_{S1}*(-d), and the unwrapped phase $\varphi_1(\sigma)$ was obtained after getting inverse Fourier transform of the windowed $F_1(d)$. The σ region in the $\varphi_1(\sigma)$ was from 1.4 μm^{-1} to 1.95 μm^{-1} in a large intensity region of $I(\sigma)$ to reduce noise effects in the $\varphi_1(\sigma)$.

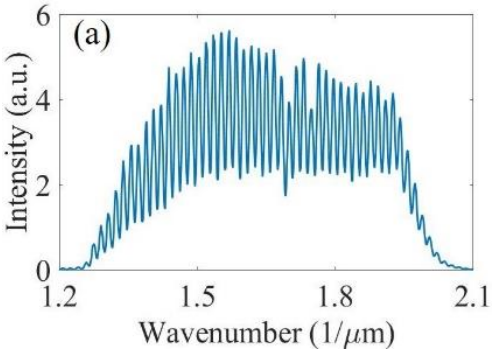

(a)

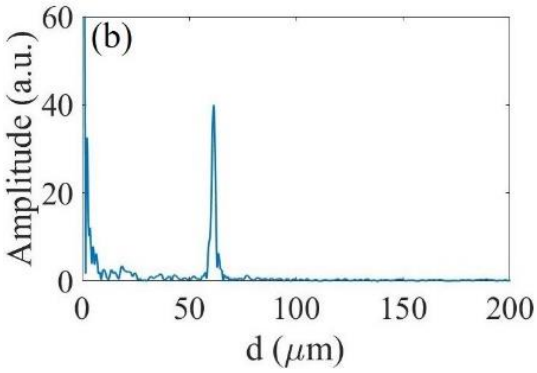

(b)

Fig. 2.8. (a) Detected interference signal $S_1(\sigma)$ and (b) amplitude distribution of its Fourier transform $F_1(d)$.

In step 2, the PZT stage was moved and stopped at a position Z_2=1587.0 μm, which compensated the increase of the optical path by a_1T. Detected signal $S_2(\sigma)$ and the amplitude distribution of Fourier transform $F_2(d)$ of $S_2(\sigma)$ are the same as Figs. 2.4 and 2.5, respectively. Windowed $F_2(d)$ was made by a rectangle window from 66 μm to 157 μm to select the component of $F_{S2}^*(-d)$ from $F_2(d)$, and inverse Fourier transform was performed on the windowed $F_2(d)$ to get the unwrapped phase $\varphi_2(\sigma)$. The d_{S2} was -102 μm, which agreed with the theoretical value of $d_{S2}=2(Z_F-a_1l_\varepsilon+a_1T-Z_2)=2(-31+1.54\times1017.4-1587)=-102$ μm, where a measured value of T=1017.4 μm was used.

In step 3 and step 4, the amplitude distributions of $F_3(d)$ and $F_4(d)$ were detected as shown in Fig. 2.9 (a) and (b), respectively. In step 3, the RS2 was used in the object arm and the PZT stage was moved to position Z_3=11935.0 μm. In Fig. 2.9 (a) the values of $W_I/2+W_{N3}$, W_{S3}, and d_{S3} were about 60 μm, 65 μm, and -98 μm, respectively. From $d_{S3}=2(Z_{R2}-a_1l_\varepsilon+(a_1-1)T-Z_3)=2(Z_{R2}-31+549-11935)=-98$ μm, Z_{R2}=11368 μm was obtained. In step 4, the PZT stage was moved back to position Z_4=11366.0 μm because the OB was

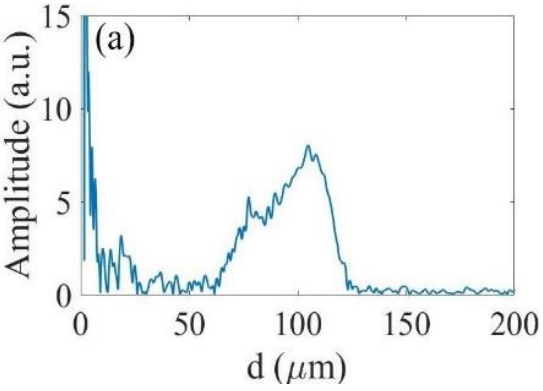

(a)

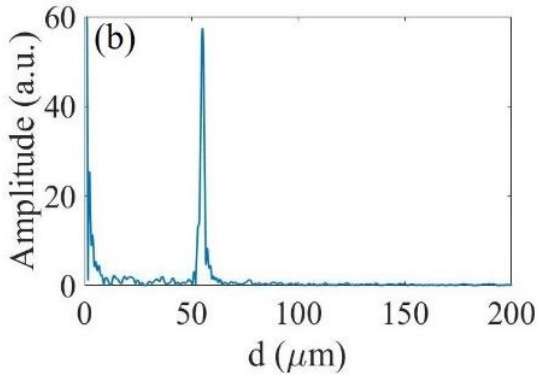

(b)

Fig. 2.9. Amplitude distribution of Fourier transform of the interference signal detected in (a) step 3 and (b) step 4.

Table. 2.1. Values in measurement of case 1.

Step	Z_i(μm)	d_{Si}(μm)	W_{Si}(μm)	Obtained values
1	0.0	-62	13	l_ε=20 μm from W_{S1} Z_F=0 μm from d_{S1}
2	1587.0	-102	67	d_{S2}= theoretical value
3	11935.0	-98	65	Z_{R2}=11368 μm from d_{S3}
4	11366.0	-56	13	$d_{S4}\cong$ theoretical value

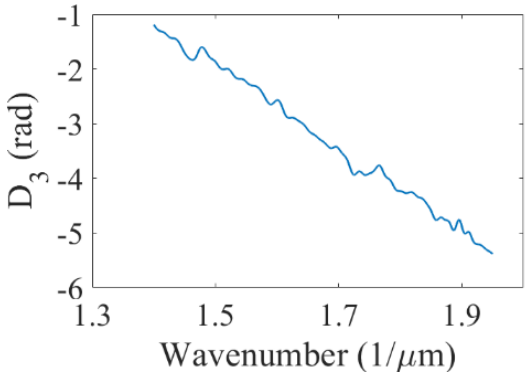

Fig. 2.10. $D_3(\sigma)$ calculated from $\varphi_1(\sigma)$ to $\varphi_4(\sigma)$ in case 1.

removed from the object arm. The values of $W_I/2+W_{N4}$ and W_{S4} were about 25 μm and 13 μm, respectively. The d_{S4} was -56 μm, which almost agreed with $d_{S4}=2(Z_{R2}-a_1 l_\varepsilon-Z_4)=2(11368-31-11366)=-58$ μm. These results described above are shown at Table 2.1 as values in measurement of case 1, and the amplitude distributions of $F_i(d)$ (i=1 to 4) have been provided in Figs. 2.8 (b),

2.5, 2.9 (a), and 2.9 (b), respectively. Distribution of $D_3(\sigma)$ obtained from $\varphi_1(\sigma)$ to $\varphi_4(\sigma)$ is shown in Fig. 2.10. The distribution of $D_3(\sigma)$ was a straight line with small fluctuations generated by noise components in $\varphi_1(\sigma)$ to $\varphi_4(\sigma)$. It is estimated that the main source of these noise components were produced by the mechanical vibrations of the interferometer and electronics noise of the spectral analyzer. In order to reduce noise effects, the least square method was used to calculate the slope of $D_3(\sigma)$ in the region of from 1.4 μm^{-1} to 1.95 μm^{-1} corresponding to a large intensity region of $I(\sigma)$. The values of $slope[D_3(\sigma)]/4\pi$ are given by Table 2.2, where the measurement was repeated three times as case 1 to case 3. It is estimated that the differences in the values of $slope[D_3(\sigma)]/4\pi$ were caused by a position change of Z_{R2} due to removing the OB between step 3 and step 4 and the 10 nm positioning repeatability of the PZT stage. In addition, the value of Z_1-Z_2+Z_3-Z_4 was regarded to be a constant value of -1018.000 μm in Eq. (2.16). The three measured values of T were a little different by less than 55 nm as shown in Table 2.2.

Table. 2.2. Measured values in case 1 to 3.

(μm)	Case1	Case2	Case3
Z_1-Z_2+Z_3- Z_4	-1018.000	-1018.000	-1018.000
$Slope\{D_3(\sigma)\}/4\pi$	-0.603	-0.618	-0.563
T	1017.397	1017.382	1017.437

2.3. Conclusion

The interference signal having the signal position was analyzed for measuring a large thickness of glass plate with the SRI using the spectral analyzer with a low resolution of 0.5 nm and the supercontinuum light source with a large bandwidth of about 300 nm. It was confirmed that the amplitude distribution of the signal component produced by the glass plate is not symmetric about the signal position which is the center of the spread width of the signal component. A measurable maximum thickness was derived by considering the resolution of the spectral analyzer and the signal component produced by the glass plate. In the four-step measurement the four spectral phase distributions of the interference signals were calculated through selecting the required signal components and doing inverse Fourier transform, and the thickness of glass plate could be obtained from the slope of the spectral phase distribution which does not contain the refractive index of glass plate. Also the positions of the reference surface 2 and the front surface of the glass plate and a dispersion effect of beam splitter were obtained from the signal components. And it was confirmed that the detected values of the signal positions agreed with the theoretical ones. A small measurement error of 50 nm was achieved in the measurement of 1 mm thickness of the glass plate.

CHAPTER 3

MORE LARGER THICKNESS MEASUREMENT USING A COMPENSATION GLASS WHOSE REFRACTIVE INDEX IS KNOWN

3.1. Introduction

A method to measure a glass plate whose thickness less than about 2 mm is described in chapter 2 [C3.5]. Thickness measurement of samples with spectrally resolved interferometer (SRI) has been reported in many papers [C3.1-C3.3, C3.5, C3.6]. Generally, optical path difference (OPD) in SRI is detected from a peak position in the amplitude distribution of Fourier transform of the interference signal for thickness measurement [C3.1-C3.2]. In order to detect OPD more exactly spectral phase of the interference signal is utilized in thickness measurement [C3.3-C3.5]. The maximum measureable thickness in chapter 2 is determined by the spread width of the amplitude distribution in Fourier transform of the interference signal. In order to reduce this spread width generated by dispersion effect due to the term of $n(\sigma)T$, a compensation glass (CG) is required for more larger thickness measurement.

In this chapter, a SRI using a CG and two positions of the RS is proposed to measure thickness larger than two millimeters. The two positions of RS are needed to detect two interference signals from front and rear surface of an OB of glass plate. First the interference signal generated from the front surface and the RS is detected. Next a CG is put into the reference arm to eliminate dispersion effect of the OB, and an interference signal generated from the rear surface and the RS is detected by changing the position of the RS with a PZT stage to make a short OPD. The positions of the RS are obtained from a controller of the PZT stage. Spectral phases of the interference signals are calculated through Fourier transform, and nonlinear components of spectral phase is utilized to obtain a difference in thickness between the OB and the CG. Thickness of the OB is obtained by calculating linear component of spectral phase which contains a linear component generated by the difference in thickness between the OB and the CG. Measurement errors less than 800 nm and 2 μm are achieved for 1 mm and 5 mm-thickness glass plates, respectively.

3.2. Principle

Figure 3.1 shows a SRI where a beam from a light source is divided by a BS for an object arm and a reference arm. The object arm contains the OB. The reference arm contains a compensation glass (CG), reference surface (RS), and a piezoelectric transducer (PZT) stage. The two beams reflected from the OB and the RS are combined by the BS and detected by a spectral analyzer as an interference signal. Thickness of the OB can be measured by two steps as shown in Figs. 3.1 (a) and (b). In step 1, the CG is not in the reference arm and the position of the front surface of OB is Z_F. An interference signal generated by the front surface of OB and the RS is detected by moving the RS to a position Z_1. In step 2, the CG is put into the reference arm to eliminate

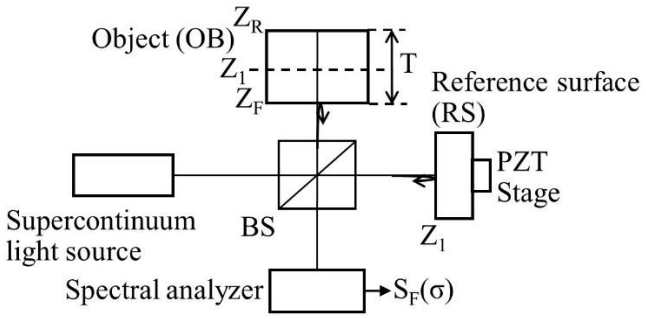

(a) step 1

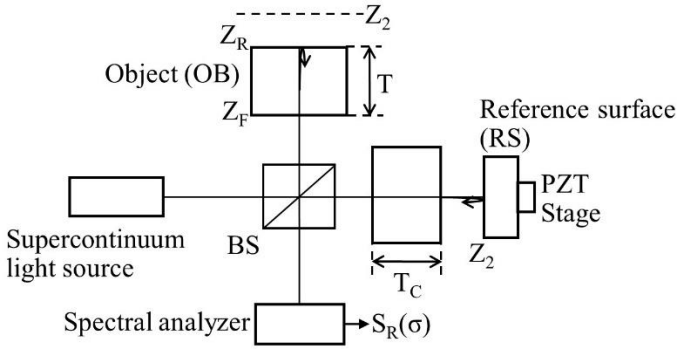

(b) step 2

Fig. 3.1. Spectral resolved interferometer whose configurations are (a) and (b) in step 1 and step 2, respectively.

dispersion effect caused by the OB. Thicknesses of the OB and the CG are T and T_C, respectively. The position of the rear surface of OB is Z_R. The RS is moved to a position Z_2 from the position Z_1 to detect an interference signal generated by the rear surface of OB and the RS. The lengths of the two sides in the BS with refractive index $n_B(\sigma)$ are different by ℓ_ε, and an optical path difference (OPD) of $2n_B(\sigma)\ell_\varepsilon$ exists between the two beams reflected from the

object and reference arms, respectively. The refractive index of the OB and the CG is $n(\sigma)$.

In step 1, the optical path difference (OPD) generated by the front surface of OB and the RS is equal to $2[Z_1\text{-}Z_F+n_B(\sigma)\ell_\varepsilon]$. The spectrally resolved interference signal is expressed as

$$S_F(\sigma) = C_F I(\sigma) + I(\sigma)\cos\{4\pi[Z_1 - Z_F + n_B(\sigma)l_\varepsilon]\sigma\}, \quad (3.1)$$

where $I(\sigma)$ is the spectral intensity of light source and σ is wavenumber and C_F is a constant value. In Fourier transform of $S_F(\sigma)$ the first term $C_F I(\sigma)$ produces low frequency components, and the second term produces high frequency components. By performing inverse Fourier transform for the positive and high frequency components in Fourier transform of $S_F(\sigma)$, the phase distribution $\varphi_F(\sigma)$ is obtained as

$$\varphi_F(\sigma) = 4\pi[(Z_1 - Z_F) + n_B(\sigma)l_\varepsilon]\sigma. \quad (3.2)$$

In step 2, the CG is put into the reference arm, and the RS moves to the position Z_2. In this step, the OPD is equal to $2[Z_2\text{-}Z_R+n(\sigma)\ell_\varepsilon+[n(\sigma)\text{-}1]T_S]$, where $T_S=T\text{-}T_C$. The spectrally resolved interference signal is expressed as

$$S_R(\sigma) = C_R I(\sigma) + I(\sigma)\cos\{4\pi[Z_2 - Z_R + n_B(\sigma)l_\varepsilon - (n(\sigma)-1)T_S]\sigma\}. \quad (3.3)$$

In the same way as $\varphi_F(\sigma)$, the phase distribution $\varphi_R(\sigma)$ of $S_R(\sigma)$ is obtained as

$$\varphi_R(\sigma) = 4\pi[Z_2 - Z_R + n_B(\sigma)l_\varepsilon - (n(\sigma)-1)T_S]\sigma. \quad (3.4)$$

The following phase distribution is calculated from Eqs. (3.2) and (3.4):

$$\varphi(\sigma) = \varphi_F(\sigma) - \varphi_R(\sigma) = 4\pi[Z_1 - Z_F - Z_2 + Z_R + (n(\sigma)-1)T_S]\sigma. \quad (3.5)$$

The phase distribution $\varphi(\sigma)$ contains a linear component and a nonlinear component. Denoting these components by $\text{linear}\{f\}$ and $\text{nonlinear}\{f\}$ in a phase distribution f, the following equation holds:

$$\varphi(\sigma) = linear\{\varphi(\sigma)\} + nonlinear\{\varphi(\sigma)\}. \quad (3.6)$$

Linear component of $\varphi(\sigma)$ expressed by $a_1\sigma+a_0$ can be obtained by calculating a least square line in $\varphi(\sigma)$. Nonlinear component of $\varphi(\sigma)$ is equal to $\text{nonlinear}\{n(\sigma)T_S\sigma\}$, and it is extracted by subtracting the linear component of $\varphi(\sigma)$ from $\varphi(\sigma)$. Theoretical values of $\text{nonlinear}\{n(\sigma)T_S\sigma\}$ are calculated by using a refractive index formula of $n(\sigma)$. By finding a value of T_S that makes the following difference a minimum value, a measurement value of T_S is obtained:

$$D(T_S) = \sum_\sigma \left[nonlinear\{4\pi n(\sigma)T_S\sigma\} - nonlinear\{\varphi(\sigma)\} \right]^2. \quad (3.7)$$

When $\text{linear}\{f\}=a_1\sigma+a_0$ is calculated , it is defined that $\text{slope}\{f\}=a_1$. Since the linear component of $\varphi(\sigma)$ is equal to $4\pi[(Z_1\text{-}Z_F\text{-}Z_2+Z_R\text{-}T_S)\sigma+\text{linear}\{4\pi n(\sigma)T_S\sigma\}]$ in Eq. (3.5), $\text{slope}\{\varphi(\sigma)/4\pi\}=Z_1\text{-}Z_F\text{-}Z_2+Z_R\text{-}T_S+\text{slope}\{n(\sigma)T_S\sigma\}$. Therefore, the measurement value of T is given by

$$T = Z_R - Z_F = slope\left\{\varphi(\sigma)/4\pi\right\} + Z_2 - Z_1 + T_S - slope\left\{n(\sigma)T_S\sigma\right\}. \quad (3.8)$$

The positions Z_1 and Z_2 of the RS are the values which are given to the PZT stage, and the value of T_S is obtained from Eq. (3.7) by using the nonlinear components of $\varphi(\sigma)$.

3.2. Experiments

The interferometer shown in Fig. 3.1 was constructed. The spectrum range of supercontinuum light source was about 500 nm to 800 nm. The RS was a glass plate with a wedge angle to regard it as one reflecting surface. The OB, CG, RS, and BS were BK7 glass. Positioning resolution and repeatability of the PZT stage were 0.5 nm and 10 nm, respectively. The PZT stage controller output the position of PZT stage. The resolution of the spectrum analyzer was 0.5 nm. Spline interpolation was performed on the interference signal detected with the spectrum analyzer for changing wavelength to wavenumber whose sampling interval was 0.001 μm^{-1}. Nominal value of the thickness of OB was 1 mm. In step 1, the PZT stage was moved to the position of Z_1=-1455.00 μm. Figure 3.2 (a) shows the interference signal $S_F(\sigma)$ detected in case 1 of the measurement, where the detected region was from 1.2 μm^{-1} to

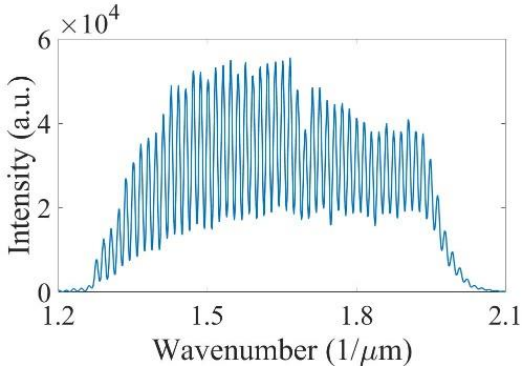

(a)

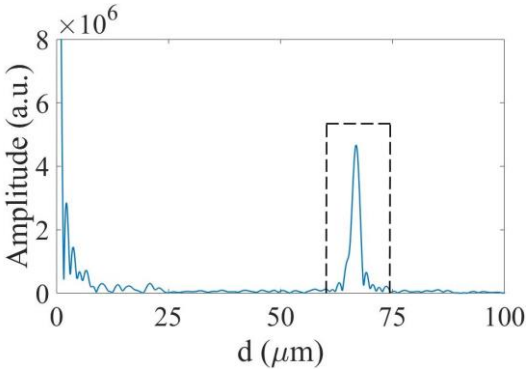

(b)

Fig. 3.2. (a) Detected interference signal of $S_F(\sigma)$, and (b) the amplitude distribution of $F_F(d)$.

2.1 μm^{-1}. Zero values were assigned outside the detected range of this interference signal to get an interference signal with a range from σ=0 μm^{-1} to σ=32.767 μm^{-1}. This wide range leaded to a sampling interval of 1/32.767=0.0305 μm in Fourier transform of the interference signal. Figure 3.2 (b) shows the amplitude distribution of $F_F(d)$, where $F_F(d)$ is the Fourier transform of $S_F(\sigma)$. The low frequency components nearby the d=0 μm was generated by $C_F I(\sigma)$ in Eq. (3.1), and the high frequency components around d=67 μm were selected by using a rectangle window from 60 μm to 74 μm indicated by dot line. After inverse Fourier transform of the windowed $F_F(d)$, The unwrapped phase of $\varphi_F(\sigma)$ was obtained from inverse Fourier transform of the windowed $F_F(d)$. In step 2, the PZT stage was moved to the position of Z_2=-430.00 μm, and the CG was put into the reference arm. Figure 3.3 (a) and (b) show the detected $S_R(\sigma)$, and the amplitude of Fourier transform of $S_R(\sigma)$, respectively. A windowed $F_R(d)$ was obtained by a rectangle window from 52 μm to 66 μm indicated by dot line. The unwrapped phase of $\varphi_R(\sigma)$ was obtained by the same method as $\varphi_F(\sigma)$. Figure 3.4 (a) shows the distribution

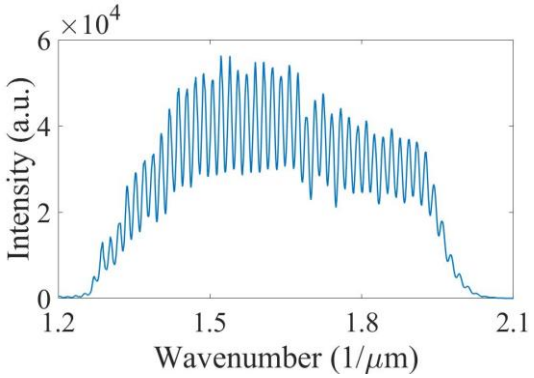

(a)

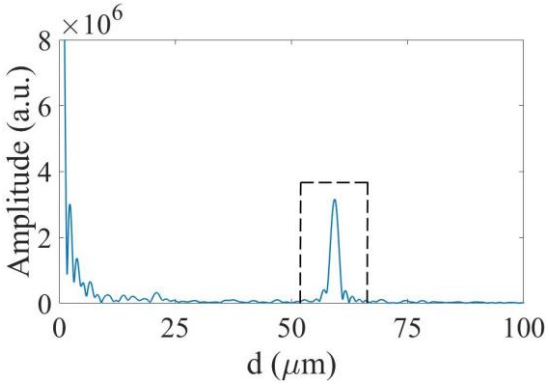

(b)

Fig. 3.3. (a) Detected interference signal of $S_R(\sigma)$, and (b) the amplitude distribution of $F_R(\sigma)$.

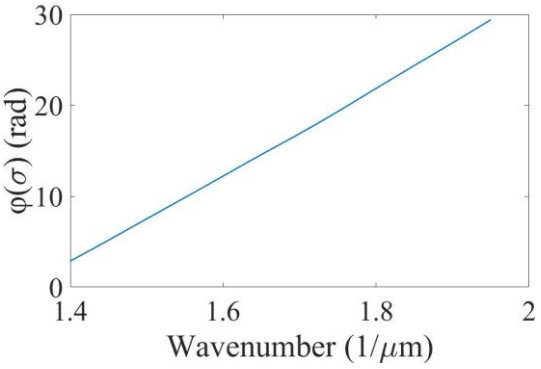

(a)

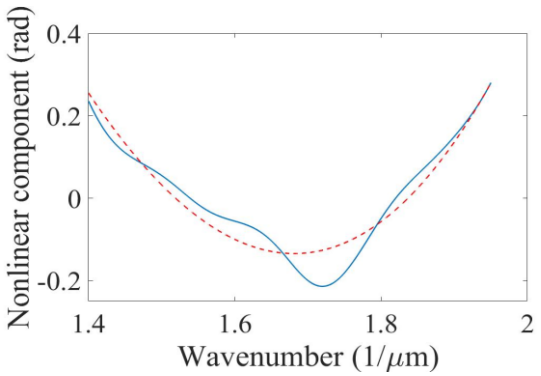

(b)

Fig. 3.4. Distributions of (a) $\varphi(\sigma)$, and (b) nonlinear$\{\varphi(\sigma)\}$ (blue curve) and nonlinear$\{4\pi n(\sigma)T_S\sigma\}$ at T_S=21.72 μm (red curve).

of $\varphi(\sigma)=\varphi_F(\sigma)-\varphi_R(\sigma)$ given by Eq. (3.5), and slope$\{\varphi(\sigma)/4\pi\}$=3.83 μm was calculated. The blue curve shown in Fig. 3.4 (b) is the nonlinear$\{\varphi(\sigma)\}$ calculated by subtracting linear$\{\varphi(\sigma)\}=4\pi\times3.83\sigma$-64.76 rad from the $\varphi(\sigma)$ shown in Fig. 3.4 (a). Figure 3.5 shows how $D(T_S)$ changed when T_S changed with an interval of 0.02 μm, and it indicates that a minimum value of T_S=21.72 μm could be obtained with a resolution of 0.02 μm, where the refractive index $n(\sigma)$ was Sellmeier equation of BK7. The red dotted curve shown in Fig. 3.4 (b) is the distribution of theoretical nonlinear$\{4\pi n(\sigma)T_S\sigma\}$ at the estimated value of T_S=21.72 μm. The slope$\{n(\sigma)T_S\sigma\}$=33.46 μm was calculated with T_S=21.72 μm. The values of Z_2-Z_1, slope$\{\varphi(\sigma)/4\pi\}$, T_S, and slope$\{[n(\sigma)T_S\sigma\}$ measured in case 1 are shown in Table 3.1. Finally, a measured value of T=1017.09 μm was calculated with the Eq. (3.8). Values measured in case 2 and 3 are also shown in Table 3.1. The difference of measured T in the three cases was less than about 0.8 μm. The thickness of OB was changed to nominal value 5 mm, and the nonlinear component of $\varphi(\sigma)$ was extracted with

the same method described for the OB of 1-mm thickness. Figure 3.6 shows the detected nonlinear$\{\varphi(\sigma)\}$ in case 1 with blue curve. A minimum value of T_S=212.00 μm was obtained by calculating $D(T_S)$ as shown in Fig. 3.7. Measured values in three cases are shown in Table 3.2, and the difference of measured T in the three cases was less than about 2 μm. Maximum difference in the measured value of T changed from 0.8 μm to 2 μm by the increase from 1 mm to 5 mm in thickness. The measured values shown in Table 3.1 and 3.2 are divided into the two components of C_1=slope$\{\varphi(\sigma)/4\pi\}+Z_2-Z_1$ and $C_2=T_S$-slope$\{n(\sigma)T_S\sigma\}$ to examine the main source of measurement error. In Table 3.1, the differences in C_1 and C_2 among the three cases are less than 0.02 μm and 0.73 μm, respectively. In Table 3.2, these differences are less than 0.14 μm and 1.96 μm. Since the difference in C_1 is much smaller than the differences in C_2, the measurement error in T depends strongly on the error in T_S estimated by nonlinear component of $\varphi(\sigma)$ containing random noise in $\varphi(\sigma)$. It is estimated that the measurement error in $\varphi(\sigma)$ is caused by mechanical vibrations of the interferometer and disturbance in air.

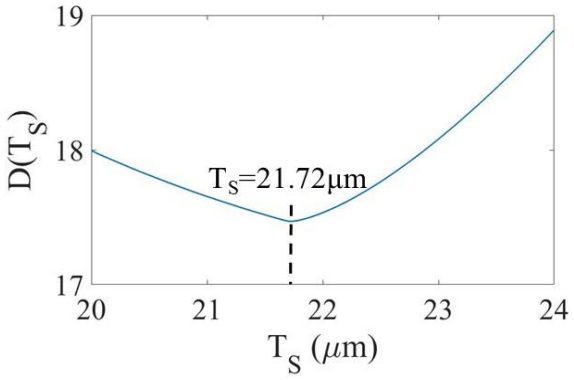

Fig. 3.5. Distribution of $D(T_S)$ versus T_S.

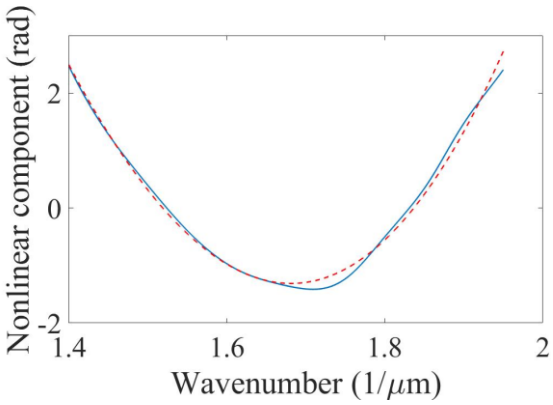

Fig. 3.6. Distributions of nonlinear$\{\varphi(\sigma)\}$(blue curve) and nonlinear$\{4\pi n(\sigma)T_S\sigma\}$ at T_S=215.50 μm (red curve) for object of 5mm-thickness.

Table. 3.1. Measured values for object of 1mm-thickness.

(μm)	Case 1	Case 2	Case 3
Z_2-Z_1	1025.00	1025.00	1025.00
slope{$\varphi(\sigma)/4\pi$}	3.83	3.83	3.85
T_S	21.72	20.36	20.90
slope{$n(\sigma)T_S\sigma$}	33.46	31.37	32.20
T	1017.09	1017.82	1017.55

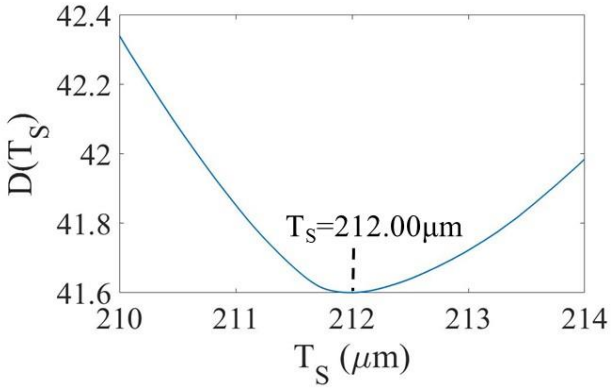

Fig. 3.7. Distribution of $D(T_S)$ versus T_S for object of 5mm-thickness.

Table. 3.2. Measured values for object of 5mm-thickness.

(μm)	Case 1	Case 2	Case 3
Z_2-Z_1	5402.00	5402.00	5402.00
slope{$\varphi(\sigma)/4\pi$}	-4.76	-4.81	-4.90
T_S	212.00	214.56	210.94
slope{$n(\sigma)T_S\sigma$}	326.60	330.54	324.96
T	5282.65	5281.21	5283.08

3.3. Conclusion

A SRI was constructed by using the spectral analyzer with a low resolution of 0.5 nm and compensation glass plates. The thickness of glass plates with 1mm and 5mm-thickness could be measured by using the spectral phase detected from the two step measurement and using the known data $n(\sigma)$ of refractive index. The nonlinear component of the detected spectral phase provided the thickness difference T_S between the OB and the CG. The linear

component generated by $[n(\sigma)-1]T_S$ was excluded from the linear component of spectral phase to calculate the thickness. The experimental results verified that the measurement error was less than 0.8 μm and 2 μm for 1 mm and 5 mm-thickness glass plates. This measurement error was mainly caused by the estimation error in T_S.

CHAPTER 4

PHASE REFRACTIVE INDEX MEASUREMENT OF GLASS PLATE TOGETHER WITH THICKNESS MEASUREMENT

4.1. Introduction

In chapters 2 and 3, thickness measurement of glass plates is achieved. Another important property of glass plate is phase refractive index. Phase refractive index of optical material has been measured by different techniques such as goniometry, ellipsometry, and reflectometry. Also interferometry is an important technique to measure phase refractive index and group refractive index. In order to measure phase or group refractive index with an interferometer, it is required to measure thickness T of an object. For these measurements a low-coherence interferometer combined with a confocal scanning microscope was used [C4.1-C4.3]. In the methods reported in Refs. C4.2 and C4.3, it is not easy to get a derivative of the scanning positions where the reflection peaks appear in the confocal scanning microscope with respect to wavenumber. Spectrally resolved interferometers (SRIs) are more useful for refractive index measurement because the interference signal of SRI is detected in wavenumber domain. It is also required to measure thickness T of an object and an optical path difference (OPD) with a SRI. However, without paying strong attentions to the measurements of thickness T and an OPD, phase refractive index $n(\sigma)$ and group refractive index $n_G(\sigma)$ have been obtained [C4.4, C4.5, C4.7-C4.9], where σ is wavenumber. In order to measure T and OPDs, different optical configurations in a SRI were employed to get group refractive index $n_G(\sigma_C)$, where σ_C is a central wavenumber in a spectral distribution of light source [C4.10-C4.14]. A peak position in the amplitude distribution of Fourier transform of the interference signal is equal to an OPD in an optical configuration of SRI. Since the peak position is related to one wavenumber of σ_C, only one value of $n_G(\sigma_C)$ is measured. Spectral phase distribution of the interference signal is better than the amplitude distribution of Fourier transform of the interference signal because the spectral phase distribution is a function of σ. Unwrapped spectral phase distribution can be calculated exactly from the interference signal through Fourier transform [C4.15,C4.16].

It is required to determine 2π phase ambiguity existing in the unwrapped phase distribution for getting phase refractive index. The unwrapped phase distribution was fitted with a polynomial function $f(\sigma)$ so that the phase ambiguity of $2\pi p$ was determined by using the relation of $f(\sigma_M)=2\pi p$, where p is an integer and the interference signal has a peak value at $\sigma=\sigma_M$

[C4.4,C4.5]. Here it is very important what kind of function is adopted as a fitting function and how the phase ambiguity is determined from the fitting. As a method without using spectral phase and a fitting function, two peak positions of a spectrally resolved interference signal generated by the two beams reflected from front and rear surfaces of an object were used to determine 2π phase ambiguity and the phase refractive index at one wavenumber [C4.6]. Another way to determine the phase ambiguity is that a phase refractive index at one wavenumber was measured with another instrument [C4.7]. In order to avoid the determination of the phase ambiguity, phase refractive index is obtained by converting measured group refractive index $n_G(\sigma)$ to phase refractive index $n(\sigma)$ by the following procedure: $n(\sigma)$ is expressed by Sellmeier equation having some coefficients, and an equation of group index is derived with the relation of $n_G(\sigma)=n(\sigma)+\sigma[\mathrm{d}n(\sigma)/\mathrm{d}\sigma]$. A measured group index is fitted to the equation of group index to determine the coefficients in Sellmeier equation of $n(\sigma)$. In this case the obtained phase refractive index is expressed by Sellmeier equation with the determined coefficients [C4.8,C4.9]. Group refractive index was measured directly from the interference signal without calculating the spectral phase distribution [C4.7,C4.8]. By differentiating the spectral phase distribution, group refractive index could be obtained eliminating the phase ambiguity [C4.9]. If an actual phase refractive index cannot be expressed exactly with the Sellmeier equation, the measurement method reported in Refs. C4.8 and C4.9 does not provide the actual phase refractive index.

The aim of this chapter is to measure both thickness T and phase refractive index $n(\sigma)$ from the spectral phase distributions detected in different optical configurations. Phase ambiguity $2\pi p$ existing in the calculated spectral phase distribution is determined by fitting the spectral phase distribution with fitting functions based on Cauchy's equation. The fitting function is very important to get an exact phase ambiguity. Because a simple equation of $n(\sigma)$ is better for the fitting, Cauchy's equation with two or three terms is adopted. The phase ambiguity $2\pi p$ is determined from the fitted value at $\sigma=0$ in the fitting function. This determination is more easy and exact than that in Refs. C4.4, C4.5, and C4.6. An actual refractive phase index $n(\sigma)$ can be obtained from a detected spectral phase distribution, a measured thickness, and the determined phase ambiguity $2\pi p$. In experiments a phase refractive index of quartz glass plate with 20 μm thickness is measured from three spectral phase distributions detected in two different optical configurations. Since there is a high possibility that the phase ambiguity cannot be correctly determined when there is a large difference between a function of real refractive index and Cauchy's equation, characteristics of the two different fitting functions are examined in experiments and discussion.

4.2. Principle

4.2.1. Detected phase distributions and thickness measurement

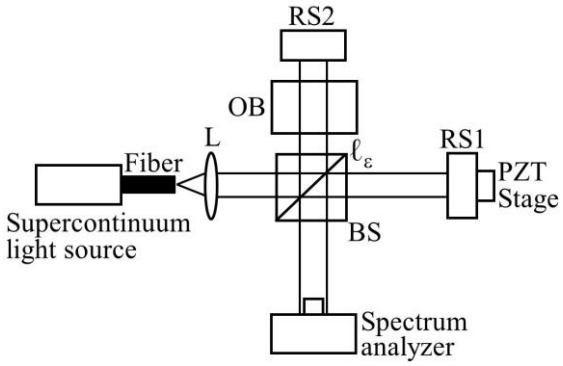

Fig. 4.1. Schematic configuration of a SRI.

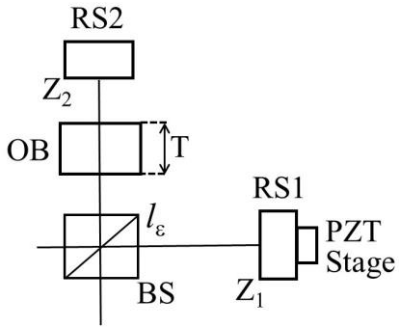

(a)

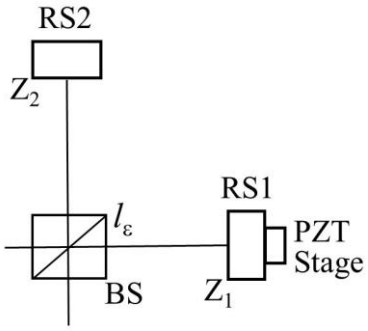

(b)

Fig. 4.2. Configuration in (a) step1 and (b) step2 for two-step measurements.

Figure 4.1 shows a schematic configuration of a SRI with a supercontinuum light source. In the reference arm a reference surface 1 (RS1) is fixed on a PZT stage. Reference surface 2 (RS2) and an OB exist in the object arm. A beam passing through a fiber is collimated with a lens, and the collimated beam is divided by a BS for the object and reference arms. The lengths of two

sides of the BS is different by a length l_ε and the refractive index of BS is $n_B(\sigma)$, where σ is wavenumber. Interference signal is detected with a spectrum analyzer. Refractive index measurement and thickness measurement are made through two measurement steps as shown in Fig. 4.2. In step 1 the OB exists in the object arm. The refractive index and the thickness of the OB are $n(\sigma)$ and T, respectively. The positions of RS1 and RS2 are Z_1 and Z_2, respectively. Two different interference signals are detected at the same time. One interference signal $S_1(\sigma)$ is produced by the two beams reflected from the front and rear surfaces of the OB, and another one $S_2(\sigma)$ is produced by the two beams reflected from the RS1 and the RS2. The two interference signals are expressed as

$$S_1(\sigma) = I(\sigma)\cos\left[4\pi n(\sigma)T\sigma + \pi\right], \tag{4.1}$$

$$S_2(\sigma) = I(\sigma)\cos\left\{4\pi\left[n_B(\sigma)l_\varepsilon + Z_1 - Z_2 - \left(n(\sigma)-1\right)T\right]\sigma\right\}, \tag{4.2}$$

where $I(\sigma)$ is the spectral intensity of light source. The value of π in signal $S_1(\sigma)$ is generated due to the beam reflected by the front surface of OB. The interference signal detected at step 1 is the summation of $S_1(\sigma)$ and $S_2(\sigma)$. Fourier transforms of $S_1(\sigma)$ and $S_2(\sigma)$ are denoted by $F_1(f)$ and $F_2(f)$, respectively. The distance of Z_1-Z_2 is required to separate $F_1(f)$ and $F_2(f)$ in frequency domain f. Inverse Fourier transform of a windowed $F_1(f)$ in the region of positive frequencies is given by

$$S_{F1}(\sigma) = I(\sigma)\exp\left[j4\pi n(\sigma)T\sigma + j\pi\right]. \tag{4.3}$$

The phase distribution $\varphi_{T1}(\sigma)$ of $S_{F1}(\sigma)$ is equal to $4\pi n(\sigma)T\sigma+\pi$ which is called theoretical phase. The theoretical phase actually obtained from fast Fourier transform is wrapped within the region from –π to π. Figure 4.3 shows schematically the theoretical phase $\varphi_{T1}(\sigma)$, the wrapped phase of $\varphi_{T1}(\sigma)$, and unwrapped phase $\varphi_{M1}(\sigma)$ by using blue, dark, and red linear lines, respectively The wrapped phase of $\varphi_{T1}(\sigma)$ is represented by dark dotted lines in the region of σ from 0 to σ_P. The dark solid lines represent the wrapped phase of $\varphi_{T1}(\sigma)$ from $\sigma=\sigma_P$. It is assumed that the detected phase $\varphi_{M1}(\sigma)$ is the same as the wrapped theoretical phase $\varphi_{T1}(\sigma)$ Actually the phase $\varphi_{M1}(\sigma)$ is not detected in the region of σ from 0 to σ_p as indicated by black dotted lines. The phase $\varphi_{M1}(\sigma)$ is unwrapped from $\sigma=\sigma_S$. The blue solid line has a value of π at σ=0 because of $\varphi_{T1}(\sigma)=4\pi n(\sigma)T\sigma+\pi$. On the other hand, the wrapped theoretical phase $\varphi_{T1}(\sigma)$ at σ=0 is regarded as -π as shown in Fig. 4.3. One period of wrapped $\varphi_{T1}(\sigma)$ is defined as the phase change from -π to π. The difference between the first period of wrapped $\varphi_{T1}(\sigma)$ and $\varphi_{T1}(\sigma)$ is equal to 2π, and this difference is increased by σ increasing. In the region from $\sigma=\sigma_P$ to σ_Q the unwrapped phase $\varphi_{M1}(\sigma)$ has the phase ambiguity of $2\pi p_1$. Then a positive integer p_1 is given by

$$p_1 = \mathrm{INT}\left\{\varphi_{T1}(\sigma_S)/2\pi\right\}, \tag{4.4}$$

where $\mathrm{INT}\{y\}$ means rounding y to the nearest integer. Thus the unwrapped

phase $\varphi_{M1}(\sigma)$ is expressed as

$$\varphi_{M1}(\sigma) = \varphi_{T1}(\sigma) - 2\pi p_1 = 4\pi n(\sigma) T\sigma + \pi - 2\pi p_1 . \quad (4.5)$$

Through the same processing as in $S_1(\sigma)$, $S_{F2}(\sigma)$ is obtained as

$$S_{F2}(\sigma) = I(\sigma)\exp\left\{ j4\pi\left[n_B(\sigma) l_\varepsilon + Z_1 - Z_2 - \left(n(\sigma)-1\right)T \right]\sigma \right\} . \quad (4.6)$$

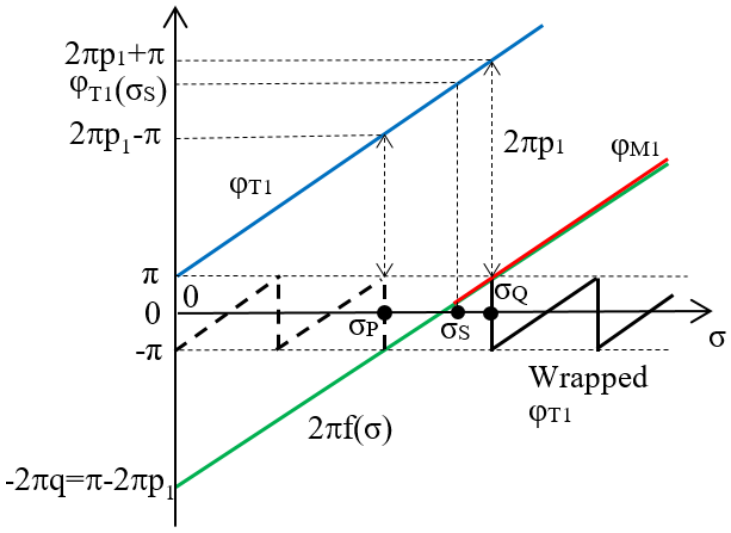

Fig. 4.3. Schematic representations of theoretical phase $\varphi_{T1}(\sigma)$, wrapped phase of $\varphi_{T1}(\sigma)$, and phase $\varphi_{M1}(\sigma)$ unwrapped from σ_S. Schematic interpretation of fitting function $2\pi f(\sigma)$.

In the same way as $\varphi_{M1}(\sigma)$, phase $\varphi_{M2}(\sigma)$ unwrapped from $\sigma=\sigma_S$ is given by

$$\varphi_{M2}(\sigma) = 4\pi[n_B(\sigma) l_\varepsilon + Z_1 - Z_2 - (n(\sigma)-1)T]\sigma - 2\pi p_2 . \quad (4.7)$$

In step 2, the OB is removed from the object arm, and the following interference signal is produced by the beams reflected from the RS1 and the RS2:

$$S_3(\sigma) = I(\sigma)\cos\left\{ 4\pi\left[n_B(\sigma) l_\varepsilon + Z_1 - Z_2 \right]\sigma \right\} . \quad (4.8)$$

Phase $\varphi_{M3}(\sigma)$ unwrapped from $\sigma=\sigma_S$ is given by

$$\varphi_{M3}(\sigma) = 4\pi[n_B(\sigma) l_\varepsilon + Z_1 - Z_2]\sigma - 2\pi p_3 . \quad (4.9)$$

In order to eliminate the term of $n(\sigma)T$ from $\varphi_{M1}(\sigma)$ and the term of $n_B(\sigma)l_\varepsilon+Z_2-Z_1$ from $\varphi_{M2}(\sigma)$, phase distribution $\varphi_{M4}(\sigma)$ is obtained as

$$\varphi_{M4}(\sigma) = \varphi_{M1}(\sigma) + \varphi_{M2}(\sigma) - \varphi_{M3}(\sigma) = 4\pi T\sigma + \pi - 2\pi p_4 . \quad (4.10)$$

Finally a value of T can be obtained from the slope of $4\pi T$ in the phase distribution $\varphi_{M4}(\sigma)$.

4.2.2. Refractive index measurement by determination of p_1

In order to determine the integer value of p_1 in the unwrapped phase distributions of $\varphi_{M1}(\sigma)/2\pi=2Tn(\sigma)\sigma+0.5-p_1$, its distribution is fitted in a region R_σ from σ_S to σ_E by a fitting function. In a fitting function, refractive index is regarded to be expressed by Cauchy's equation

$$n(\sigma) = b_0 + b_2\sigma^2 + b_4\sigma^4 + \dots . \tag{4.11}$$

Thus the fitting function is given by

$$f(\sigma) = 2Tn(\sigma)\sigma + 0.5 - p_1 = 2T(b_0\sigma + b_2\sigma^3 + b_4\sigma^5 + \dots) - q . \tag{4.12}$$

Figure 4.3 shows schematically this fitting situation where $f(0)=-q=0.5-p_1$ under the condition of $\varphi_{M1}(\sigma)/2\pi=f(\sigma)$. The $2\pi f(\sigma)$ is represented by green line. It is expected that value of p_1 is obtained from fitting $\varphi_{M1}(\sigma)/2\pi$ with the fitting function of Eq. (4.12). When the experimental data of $\varphi_{M1}(\sigma)/2\pi$ cannot be exactly expressed by the fitting equation, the value of $q+0.5$ obtained from the fitting is not equal to the integer value p_1. In many cases the integer value of p_1 can be decided by rounding the value of $q+0.5$. By using the measured T value and the decided p_1 value the following refractive indexes $n_1(\sigma)$ is obtained from $\varphi_{M1}(\sigma)$:

$$n_1(\sigma) = \frac{\varphi_{M1}(\sigma) - \pi + 2\pi p_1}{4\pi T\sigma} . \tag{4.13}$$

4.3. Simulations

4.3.1. Unwrapped data of phase distribution

Figure 4.4 shows the spectral intensity $I(\sigma)$ of light source detected in experiments. In order to reduce effects of noises, the region of R_σ for the fitting was decided by selecting a region of large intensity $I(\sigma)$ as shown in Fig. 4.4, where σ_S=1.4 μm^{-1} and σ_E=1.95 μm^{-1}. Unwrapped phase data of $\varphi_{M1}(\sigma)/2\pi=2Tn(\sigma)\sigma+0.5-p_1$ expressed with Eq. (4.5) was made by using the

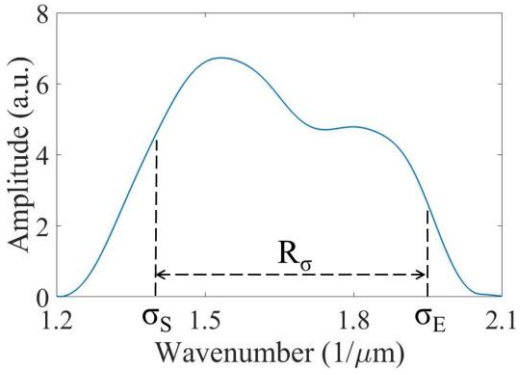

Fig. 4.4. Spectral intensity $I(\sigma)$ of light source detected in experiments.

refractive index of Cauchy's equation. Coefficients of Cauchy's equation were obtained by fitting the refractive index $n_S(\sigma)$ of Sellmeier equation of quartz glass with $n_{C1}(\sigma)= b_0+b_2\sigma^2$ and $n_{C2}(\sigma)= b_0+b_2\sigma^2+b_4\sigma^4$ in the region R_σ. The refractive index $n_S(\sigma)$ of quartz glass was given by $n_S^2(\sigma)=1+\sum_{i=1}^{3}\frac{B_i}{1-C_i\sigma^2}$, where B_1=0.6962, B_2=0.4079, B_3=0.8975, C_1=0.0047, C_2=0.0135, C_3=97.9340 [C4.17]. The fitted coefficients b_i (i=0, 2, 4) and root-mean-square of difference (RMSD) between $n_S(\sigma)$ and $n_{C1}(\sigma)$ or $n_{C2}(\sigma)$ are shown in Table 4.1. Since the refractive index $n_{C2}(\sigma)$ with the fitted coefficients has the smaller RMSD, $n_{C2}(\sigma)$ was used as $n(\sigma)$ to make the interference signal data of $S_1(\sigma)$ given by Eq. (4.1) where a thickness of T=20.073 μm measured in experiments was used. Since the values of $\varphi_{T1}(\sigma_S)/2\pi=2Tn_{C2}(\sigma_S)\sigma_S+0.5$ was equal to 82.28 in Eq. (4.4), the value p_1 was estimated to be 82.

Table. 4.1. Results of fitting $n_S(\sigma)$ with $n_{C1}(\sigma)$ and $n_{C2}(\sigma)$.

	b_0	b_2	b_4	RMSD
$n_{C1}(\sigma)$	1.448	0.0036		3.07×10^{-5}
$n_{C2}(\sigma)$	1.447	0.0043	-0.0001	6.46×10^{-6}

4.3.2. Fitting function $f(\sigma)$

Simulations were carried out to examine characteristics of the fitting method to determine a value of p_1. The phase data of $\varphi_{M1}(\sigma)/2\pi$ was calculated from the simulated signal of $S_1(\sigma)$ through Fourier transform. The following two fitting functions given by Eq. (4.12) were made by using the values of coefficients of $n_{C1}(\sigma)$ and $n_{C2}(\sigma)$ shown in Table 4.1: $f_1(\sigma)=2T(1.448+0.0036\sigma^2)\sigma-q$ and $f_2(\sigma)=2T(1.447+0.0043\sigma^2-0.0001\sigma^4)\sigma-q$ corresponding to $n_{C1}(\sigma)$ and $n_{C2}(\sigma)$, respectively, where T=20.073 μm. Trust-Region method in Matlab was used for the fitting calculations. Results of these fittings are shown in Table 4.2. Since the simulated data of $\varphi_{M1}(\sigma)/2\pi$ was made by using the refractive index of $n_{C2}(\sigma)=1.447+0.0043\sigma^2-0.0001\sigma^4$, the results of the fitting are better in the fitting function of $f_2(\sigma)$. When the data of $\varphi_{M1}(\sigma)/2\pi=2T(1.447+0.0043\sigma^2-0.0001\sigma^4)\sigma-81.5$ was used instead of the data calculated from the simulated signal of $S_1(\sigma)$, the results of b_0=1.447, b_2=0.0043, b_4=-0.0001, and q+0.5=82.00 were obtained in the fitting with

Table. 4.2. Simulation results with the two fitting functions.

	b_0	b_2	b_4	q+0.5
$f_1(\sigma)$	1.452	0.0032		82.17
$f_2(\sigma)$	1.448	0.0041	-0.0001	82.03

$f_2(\sigma)$. This indicates that there was computation error in the phase data of $\varphi_{M1}(\sigma)/2\pi$ calculated from $S_1(\sigma)$. Both $f_1(\sigma)$ and $f_2(\sigma)$ are used in experiments to examine the characteristics of the fitting functions under the situation that the experimental data of $\varphi_{M1}(\sigma)/2\pi$ is not exactly expressed by the fitting equations.

4.4. Experiments

4.4.1. Detection of phase distributions and thickness measurement

The SRI shown in Fig. 4.1 was constructed to measure a thickness and a refractive index at one point of the object. A glass plate with wedged angle was used as one reflecting surface for RS1 and RS2. The BS1 was BK7 glass and the object was a quartz glass plate with 20 μm thickness. The spectral range of the supercontinuum light was about 500nm-800nm. The interference signals were detected by a spectrum analyzer with wavelength resolution of about 0.5 nm. Since the bit number of A/D converter in the spectrum analyzer was 16 bit, the resolution of spectral phase is estimated to be on the order of 0.01 rad. The resolutions in thickness and refractive measurements depend on this phase resolution. For converting the detected interference signal to the signal in wavenumber domain, spline interpolation was carried out with a constant interval of $0.001\mu m^{-1}$. The interference signal detected in step 1 is shown in Fig. 4.5 (a). In order to distinguish the two interference signals $S_1(\sigma)$ and $S_2(\sigma)$ contained in Fig. 4.5 (a), the distance of Z_1-Z_2 was about 17 μm. Figure 4.5 (b) shows the amplitude distribution of Fourier transform of the interference signal. Windowed $F_1(f)$ of $S_1(\sigma)$ was made by using a rectangle window existing from f=52μm to f=66μm to obtain the function $S_{F1}(\sigma)$. Another rectangle window from f=66μm to f=80μm was used to obtain the function $S_{F2}(\sigma)$. The unwrapped $\varphi_{M1}(\sigma)$ and $\varphi_{M2}(\sigma)$ in the region of R_σ from σ_S to σ_E were obtained from $S_{F1}(\sigma)$ and $S_{F2}(\sigma)$, respectively, where σ_S=1.4 μm^{-1}. In order to confirm small variations contained in the detected distribution of $\varphi_{M1}(\sigma)/2\pi$ and the value of $\varphi_{M1}(\sigma_S)/2\pi$, the distribution of $[\varphi_{M1}(\sigma)/2\pi]$-59($\sigma$-$\sigma_S$) is shown in Fig. 4.6 (a). In step 2, unwrapped phase $\varphi_{M3}(\sigma)$ was obtained

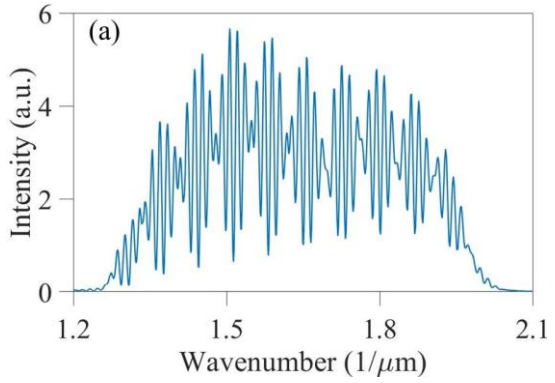

(a)

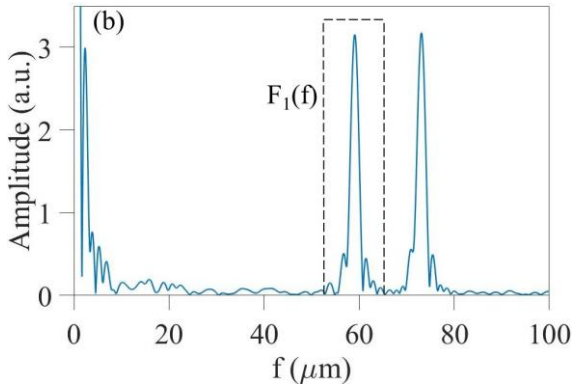

(b)

Fig. 4.5. Distribution of (a) interference signal and (b) amplitude of Fourier transform of the interference signal.

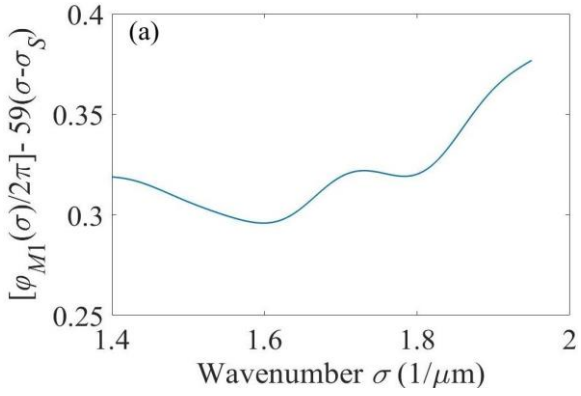

(a)

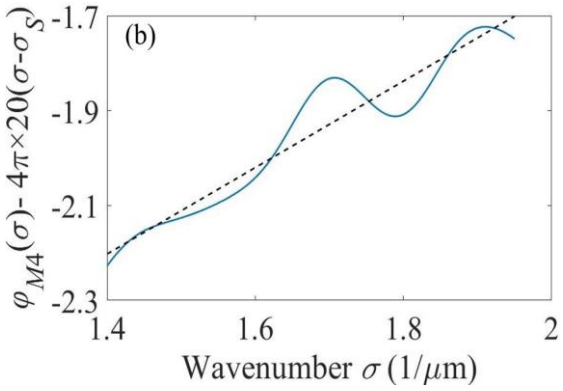

(b)

Fig. 4.6. Detected distributions of (a) $[\varphi_{M1}(\sigma)/2\pi]$-$59(\sigma-\sigma_S)$, (b) $\varphi_{M4}(\sigma)$-$4\pi\times20(\sigma-\sigma_S)$ and least square line, where σ_S=1.4 μm^{-1}.

from the interference signal $S_3(\sigma)$ with the same signal processing. Finally the phase distribution of $\varphi_{M4}(\sigma)=\varphi_{M1}(\sigma)-\varphi_{M3}(\sigma)+\varphi_{M2}(\sigma)$ given by Eq. (4.10) was obtained. Figure 4.6 (b) shows the distribution of $\varphi_{M4}(\sigma)-4\pi\times20(\sigma-\sigma_S)$ which contained small fluctuations. The slope of least square line in this distribution was 0.9111 rad×μm as shown Fig. 4.6 (b), and the slope in the $\varphi_{M4}(\sigma)$ was 0.9111+4π×20 rad×μm. Thus the measured thickness of the OB was equal to (0.9111/4π)+20=20.0725 μm. The measurement was repeated three times as Case 1, 2, and 3. The three measured values of T are shown in Table 4.3, where a maximum difference in the three cases was 6 nm. From these measured values, it is estimated that the measurement error in T was less than 6 nm.

Table. 4.3. Measured values of T in three cases.

(μm)	Case 1	Case 2	Case 3
T	20.073	20.079	20.075

4.4.2. Determination of p_1 and refractive index measurement

The detected distribution of $\varphi_{M1}(\sigma)/2\pi$ was fitted with the fitting functions of $f_1(\sigma)$ and $f_2(\sigma)$. The values of $\varphi_{M1}(\sigma)/2\pi$ changed from about 0 to 35 in the region of R_σ as shown in Fig. 4.6 (a). Difference between the distribution of $\varphi_{M1}(\sigma)/2\pi$ and the fitted distribution of $f_1(\sigma)$ or $f_2(\sigma)$ is denoted by $\Delta f_1(\sigma)$ or $\Delta f_2(\sigma)$, respectively. The results of the differences in the three cases are shown in Fig. 4.7. Since the distributions of Δf_1 and Δf_2 in each case were almost the same, the fitting in the region of R_σ was done well with the fitting functions of $f_1(\sigma)$ and $f_2(\sigma)$. The fitted values of b_0, b_2, and b_4 are shown in Table 4.4. Figure 4.8 shows distributions of the fitted $f_1(\sigma)$ and $f_2(\sigma)$ around σ=0 with red curve and blue curve, respectively, in the three cases. It is

expected that the values of $f_1(0)$=-q and $f_2(0)$ =-q are from -82 to -81 because the integer value of p_1=82 is obtained by rounding the value of q+0.5. Although $f_1(0)$ provided a good value of $-q$ in all three cases, $f_2(0)$ did not provide a good value of $-q$ except Case 1. It was made clear that the fitting function $f_2(\sigma)$ produced an incorrect fitted value at σ=0 even when the difference $\Delta f_2(\sigma)$ was not so large. Figure 4.9 shows the measured refractive index of $n_1(\sigma)$ given by Eq. (4.13) in Case 1, 2, and 3 together with $n_{C2}(\sigma)$=1.447+0.0043σ^2-0.0001σ^4, where the solid curves and the doted curve are $n_1(\sigma)$ and $n_{C2}(\sigma)$, respectively. It is indicated that the measured refractive indices are different from the $n_{C2}(\sigma)$. Figure 4.10 shows the difference in $n_1(\sigma)$

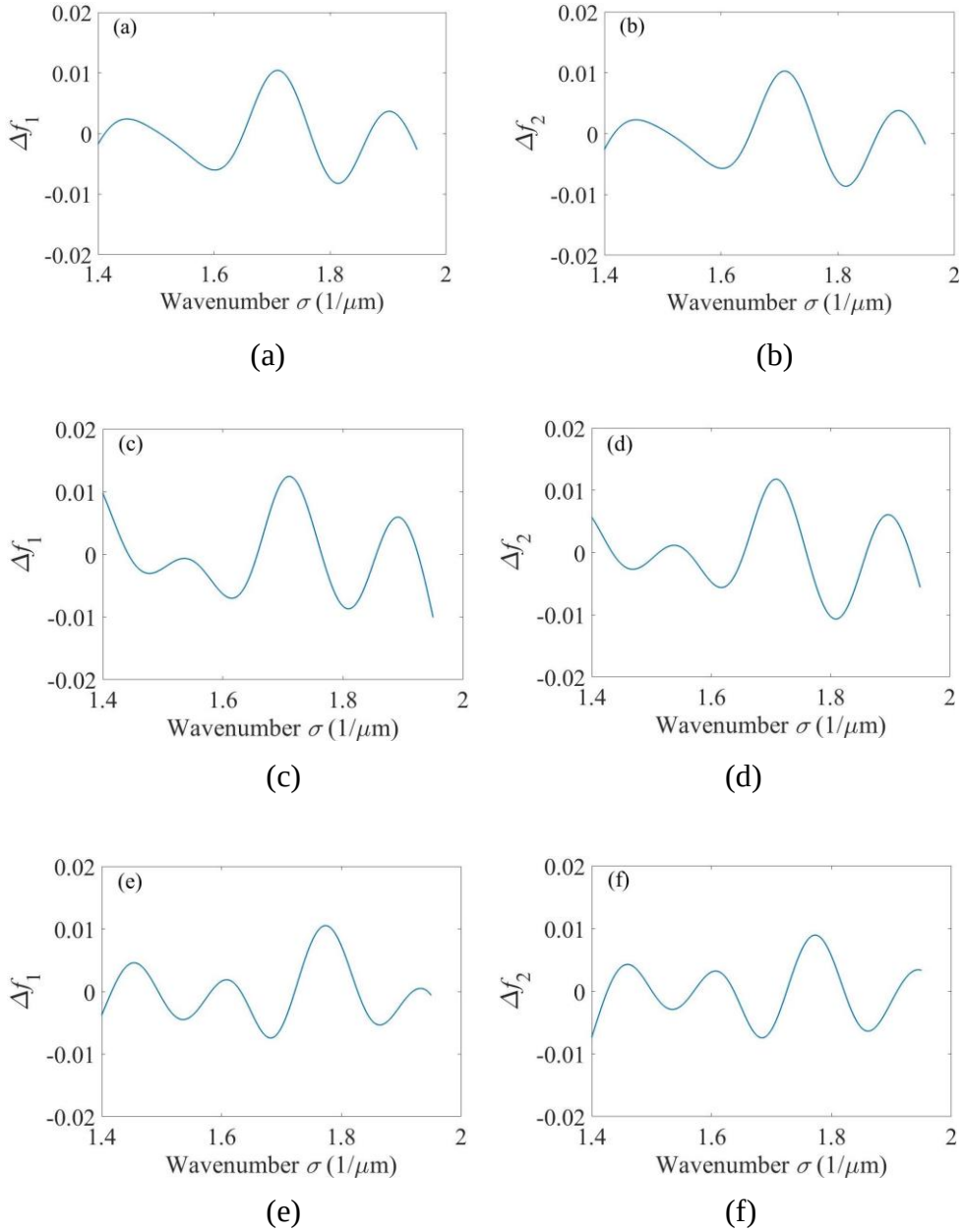

Fig. 4.7. Distributions of Δf_1=$\varphi_{M1}/2\pi$ - f_1 and Δf_2=$\varphi_{M1}/2\pi$ – f_2. (a) Δf_1 and (b) Δf_2 in Case 1, (c) Δf_1 and (d) Δf_2 in Case 2, (e) Δf_1 and (f) Δf_2 in Case 3.

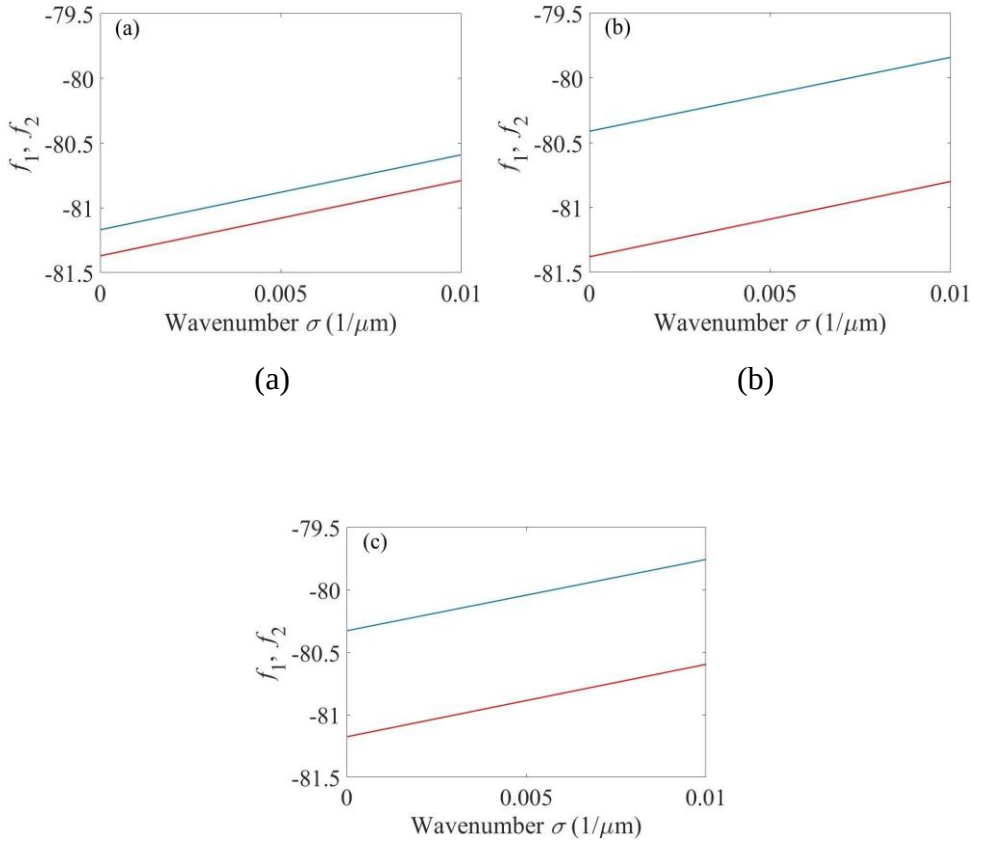

Fig. 4.8. Distributions of fitted $f_1(\sigma)$ (red curve) and $f_2(\sigma)$ (blue curve) around σ=0 in (a) Case 1, (b) Case 2, and (c) Case 3.

Table 4.4. Experimental results in three cases to obtain p_1 with two fitting functions.

	$f_1(\sigma)$			$f_2(\sigma)$		
	Case 1	Case 2	Case 3	Case 1	Case 2	Case 3
b_0	1.4478	1.4477	1.4432	1.4422	1.4203	1.4193
b_2	0.0029	0.0029	0.0034	0.0042	0.0094	0.0092
b_4				-0.0001	-0.0007	-0.0006
q+0.5	81.87	81.88	81.68	81.67	80.91	80.83
p_1	82	82	82	82	81	81

between the two cases. The blue curve is the difference between Case 2 and Case 1, and the green curve is the one between Case 3 and Case 1. It is made clearly that the refractive index can be measured with an error less than 0.0005. The sources of the measurement error are estimated to be mechanical

vibrations of the interferometer, disturbance in air, and displacements of the two reference surfaces caused by removing the object in step 2.The measured refractive index $n_1(\sigma)$ was obtained from the detected distribution $\varphi_{M1}(\sigma)$ and the fitted value p_1. Another refractive index obtained with a similar way as reported in Refs. C4.8 and C4.9 is the fitted refractive index $n_{C1}(\sigma)= b_0+b_2\sigma^2$ with the fitted values of b_0 and b_2. Figure 4.11 shows the $n_{C1}(\sigma)$ in the three cases together with $n_{C2}(\sigma)$=1.447+0.0043σ^2-0.0001σ^4. It is clear that the measured refractive index $n_1(\sigma)$ provides an actual refractive index which is more exact than the fitted refractive index $n_{C1}(\sigma)$.

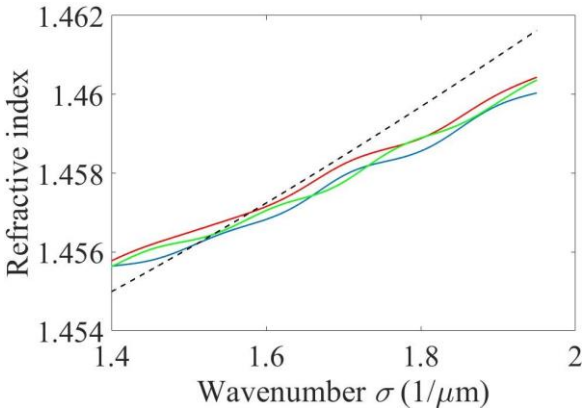

Fig. 4.9. Refractive indices $n_1(\sigma)$ in Case 1 (red curve), Case 2 (blue curve), and Case 3 (green curve). Dark dotted curve is refractive index $n_{C2}(\sigma)$=1.447+0.0043σ^2-0.0001σ^4.

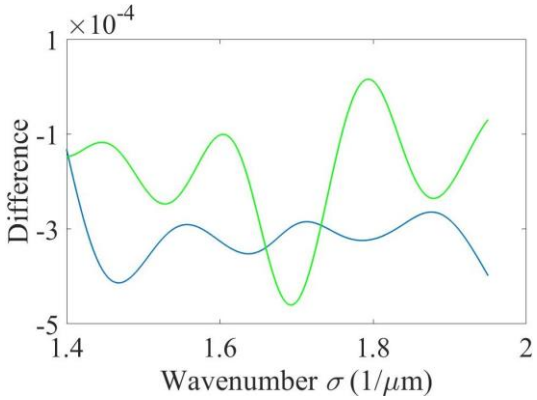

Fig. 4.10. Difference in $n_1(\sigma)$ between Case 2 and Case 1 (blue curve), and difference between Case 3 and Case 1 (green curve).

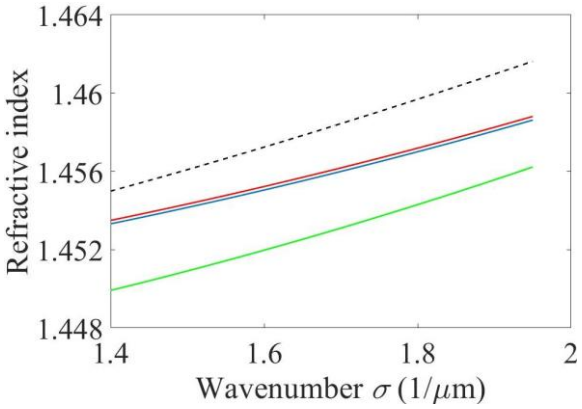

Fig. 4.11. Refractive indexes $n_{C1}(\sigma)$ using the fitted values b_0 and b_2 of $f_1(\sigma)$ in Case 1 (red curve), Case 2 (blue curve), and Case 3 (green curve). Dark dotted curve is refractive index of $n_{C2}(\sigma)$=1.447+0.0043σ^2-0.0001σ^4.

4.5. Discussion

In order to examine whether a refractive index deviating from the $n_{C2}(\sigma)$ can be measured with the fitting functions $f_1(\sigma)$ and $f_2(\sigma)$, the following refractive indexes were considered: (1) $n(\sigma)$=1.447+$b_1\sigma$+0.0043σ^2-0.0001σ^4 and (2) $n(\sigma)$=1.447+0.006σ+0.0043σ^2+$b_3\sigma^3$-0.0001σ^4. The value of b_1 or b_3 changed, and $\varphi_{M1}(\sigma_S)/2\pi=2T\mathrm{n}(\sigma_S)\sigma_S$+0.5 was calculated to obtain the value of p_1 with Eq. (4.4) where T=20.073 μm and σ_S=1.4 μm^{-1}. The unwrapped phase data of $\varphi_{M1}(\sigma)/2\pi$ was made from the interference signal $S_1(\sigma)$ given by Eq. (4.1), and the data was fitted with $f_1(\sigma)=2T(b_0+b_2\sigma^2)\sigma-q$ and $f_2(\sigma)=2T(b_0+b_2\sigma^2+\mathrm{b}_4\sigma^4)\sigma-q$. Table 4.5 shows the results obtained at the refractive index of (1) and $f_1(\sigma)$, where the fitted value of b_0, b_2, and q are shown. According to the change in the value of b_1 of $n(\sigma)$, the value of p_1 changed. It is clear by comparing q+0.5 to p_1 that the exact value p_1 can be obtained in the region of -0.018<b_1<0.010. Table 4.6 shows the results obtained at the refractive index of (1) and $f_2(\sigma)$. In this case the exact value p_1 can be obtained in the region of -0.024<b_1<0.020.

Table 4.5. Results at $n(\sigma)$=1.447+$b_1\sigma$+0.0043σ^2-0.0001σ^4 and $f_1(\sigma)$.

b_1	-0.018	-0.016	-0.012	0	0.004	0.008	0.010
$\varphi_{M1}(\sigma_S)/2\pi$	80.86	81.02	81.34	82.28	82.59	82.91	83.07
p_1	81	81	81	82	83	83	83
b_0	1.421	1.424	1.431	1.452	1.458	1.464	1.468
b_2	-0.0002	0.0002	0.0010	0.0032	0.0042	0.0049	0.0053
q+0.5	80.47	80.55	80.70	82.17	83.29	83.44	83.51

Table 4.6. Results at $n(\sigma)=1.447+b_1\sigma+0.0043\sigma^2-0.0001\sigma^4$ and $f_2(\sigma)$.

b_1	-0.024	-0.022	-0.018	0	0.014	0.018	0.020
$\varphi_{M1}(\sigma_S)/2\pi$	80.39	80.55	80.86	82.28	83.38	83.70	83.85
p_1	80	81	81	82	83	84	84
b_0	1.417	1.419	1.424	1.448	1.466	1.471	1.474
b_2	-0.0028	-0.0022	-0.0011	0.0041	0.0081	0.0093	0.0099
b_4	0.0001	0.0001	0.0001	-0.0001	-0.0002	-0.0003	-0.0003
q+0.5	79.45	80.50	80.60	82.03	83.36	84.45	84.50

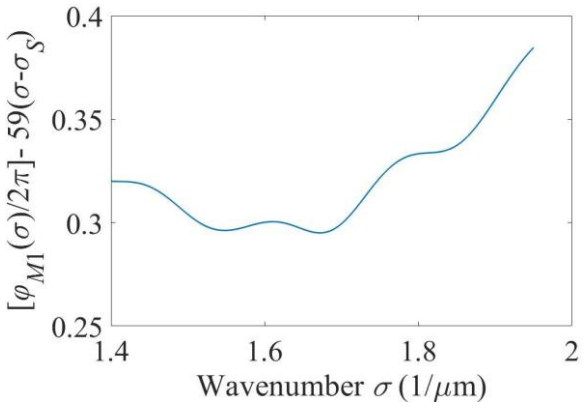

Fig. 4.12. Detected distributions of $[\varphi_{M1}(\sigma)/2\pi]$-59($\sigma$-$\sigma_S$) in Case 3.

Next the refractive index of (2) was considered, where the value of b_1 was fixed at 0.006. The regions where the exact value p_1 could be obtained with $f_1(\sigma)$ and $f_2(\sigma)$ were $-0.0006<b_3<0.003$ and $-0.007<b_3<0.006$, respectively. From these results it is made clear that the fitting function $f_2(\sigma)$ can produce an exact p_1 value than $f_1(\sigma)$ because the values of b_2 and b_4 change well according to the change in b_1 or b_3 of $n(\sigma)$. However, in the experiments the fitting function $f_2(\sigma)$ provided the exact p_1 in only Case 1 among the three cases. It is estimated that $f_2(\sigma)$ does not work well when the spectral phase distribution has small fluctuations as shown in Fig. 4.12. Comparing the phase distribution in Case 3 shown in Fig. 4.12 with that in Case 1 shown in Fig. 4.6 (a), the small fluctuations is stronger in Fig. 4.12. As a conclusion, it is better that the two fitting functions $f_1(\sigma)$ and $f_2(\sigma)$ are used for measuring refractive indexes which are expressed by functions different from Cauchy's equation.

4.6. Conclusion

A new method for measuring phase refractive index distribution of a glass plate has been proposed where the three spectral phase distributions detected in the two different optical configurations of a spectrally resolved interferometer were used to measure simultaneously both thickness and refractive index of a glass plate. The phase ambiguity $2\pi p_1$ existing in a detected unwrapped phase distribution was determined by fitting the phase distribution with two fitting functions based on Cauchy's equation. Phase refractive index distribution of a quartz glass plate with 20 μm thickness could be measured with an error less than 0.0005 from the unwrapped spectral phase distribution $\varphi_{M1}(\sigma)$, the measured thickness T, and the determined phase ambiguity p_1. It was made clear in the experiment and the discussion how the two fitting functions produced the value of p_1.

CHAPTER 5

CONCLUSIONS

In Sec.1.1, single wavelength interferometer, white light scanning interferometer (WLSI), and spectrally resolved interferometer (SRI) were explained and compared. SRI was adopted as a better interferometer for measurements of thickness and refractive index. It was explained that spectral phase containing in the interference signal as a phase term is utilized for the measurements.

Section 1.2 described how measurements of thickness and refractive index are motivated by improving the measurements with using SRI.

First in Sec.1.2.1, it was explained how a SRI is improved to measure a large thickness of glass plate with a low resolution spectral analyzer (SPA) and also how the interference signals are processed to obtain the thickness. In the five subsections from Sec.1.2.1.1 to Sec.1.2.1.5, the following methods were presented: In Sec.1.2.1.1, it was explained that a high resolution SPA is required to detect an interference signal with a small period due to a large OPD produced by a large thickness of glass plate. In order to detect the interference signal with a low resolution SPA, the position of reference surface is changed by using a high accurate PZT stage to reduce the OPD of the interference signal. In Sec.1.2.1.2, properties of different two methods to obtain the thickness from the interference signal were compared. One method is to use the peak of amplitude distribution of Fourier transform of the interference signal. Another method is to extract the spectral phase from the interference signal. It was concluded that the spectral phase is better because it is directly related to OPD. In Sec.1.2.1.3, dispersion effect caused by a cubic beam splitter (BS) was explained. Since the term of $n_B(\sigma)l_\varepsilon$ generated by the dispersion effect is contained in each spectral phase, it can be eliminated by subtraction between two different spectral phases. In Sec.1.2.1.4, it was described that the term of $n(\sigma)T$ containing in a spectral phase should be eliminated to obtain a measurement value of T. This elimination is done by subtracting two spectral phases detected in different optical configurations. In Sec.1.2.1.5, it was explained how to measure more larger thickness T which increases the dispersion effect. A compensation glass (CG) with thickness T_C is used to reduce the dispersion effect. Spectral phase $\varphi(\sigma)$ obtained from different spectral phases has a term of $n(\sigma)(T\text{-}T_C)$. A value of $T\text{-}T_C$ is estimated by using nonlinear component of $\varphi(\sigma)$. A measurement value of T can be obtained from the spectral $\varphi(\sigma)$ and the estimated value of $(T\text{-}T_C)$.

Next in Sec. 1.2.2, it was explained how a real refractive index is obtained directly from the detected spectral phase. The 2π phase ambiguity existing in a detected and unwrapped spectral phase is determined by fitting the unwrapped phase with a fitting function. An actual refractive index is

obtained from a distribution of the detected spectral phase and the determined 2π phase ambiguity.

In Sec.1.3 organization of the thesis was explained by presenting figures which show flow of measurement and connections to Chapter 2, 3, and 4.

In Chapter 2, it was made clear theoretically that the maximum measurable thickness T_m depends on the dispersion effect of glass plate. T_m was less than 2 mm when the resolution of SPA is 0.5 nm and the object is BK7 glass plate. A SRI was constructed with a SPA of 0.5 nm resolution and a PZT stage of 10 nm positioning accuracy. Experimental results showed that a small measurement error of 50 nm was achieved in the measurement of 1 mm thickness of the glass plate.

In Chapter 3, dispersion effect generated by an object of more larger thickness T was compensated by using a compensation glass (CG) plate of thickness T_C. The known refractive index of the CG and the object was the same. In experiments, the estimated values of T-T_C were 21 μm and 212 μm at objects of 1 mm and 5 mm-thickness, respectively. 1 mm and 5 mm-thickness glass plates were measured with error less than 0.8 μm and 2 μm, respectively.

In Chapter 4, it was explained how to obtain actual refractive index from the unwrapped spectral phase $\varphi_{M1}(\sigma)$. The phase ambiguity $2\pi p_1$ in $\varphi_{M1}(\sigma)$ was determined by fitting $\varphi_{M1}(\sigma)$ with a fitting function. Properties of the following two fitting functions based on Cauchy's equation were examined: $f_1(\sigma)=2T(b_0\sigma+b_2\sigma^3)+0.5-p_1$ and $f_2(\sigma)=2T(b_0\sigma+b_2\sigma^3+b_4\sigma^5)+0.5-p_1$. The simulation results showed that both $f_1(\sigma)$ and $f_2(\sigma)$ can provide a correct value of p_1 after rounding off the fitted value of p_1. On the other hand, experimental results made it clear that $f_1(\sigma)$ provides a correct value of $p_1=82$ more frequently than $f_2(\sigma)$ because the smaller number of terms in $f_1(\sigma)$ makes the fitting function non-sensitive to noise containing in the $\varphi_{M1}(\sigma)$. The measured thickness of a quartz glass plate with 20 μm thickness was 20.08 μm with error less than 6 nm. Finally a real phase refractive index distribution could be measured with an error less than 0.0005 from the detected spectral phase $\varphi_{M1}(\sigma)$, the measure thickness T, and the fitted value of p_1.

REFERENCES

Chapter 1: (C1)

[1] P. Hariharan, “Basics of interferometry,” Elsevier Academic Press, 2007, 16-17.

[2] J. Schmit, K. Creath, J. C. Wyant, “Surface Profilers, Multiple Wavelength, and White Light Intereferometry,” Optical Shop Testing, 2006, 711-716.

[3] J. Schmit, K. Creath, J. C. Wyant, “Surface Profilers, Multiple Wavelength, and White Light Intereferometry,” Optical Shop Testing, 2006, 731-735.

[4] J. Na, H. Y. Choi, E. S. Choi, C. Lee, and B. H. Lee, “Self-referenced spectral interferometry for simultaneous measurements of thickness and refractive index,” Applied Optics, 2009, **48**(13), 2461-2467.

[5] S. J. Park, K. S. Park, Y. H. Kim, and B. H. Lee, “Simultaneous Measurements of Refractive Index and Thickness by Spectral-Domain Low Coherence Interferometry Having Dual Sample Probes,” IEEE Photonics Technology Letters, 2011, **23**(15), 1076-1078.

[6] S. Luo, O. Sasaki, Z. Chen, and J. Pu, “Utilization of complex-valued signals in a white-light scanning interferometer for accurate measurement of a surface profile,” Applied Optics, 2017, **56**(15), 4419-4425.

[7] Y. Ghim, H. Rhee, H. Yang, and Y. Lee, “Thin-film thickness profile measurement using a Mirau-type low-coherence interferometer,” Measurement Science and Technology, 2013, **24**(7), 705002.

[8] Y. Arosa, and R. Fuente, “Evaluation of group index in spectrally resolved white light interferometry,” Optics & Laser Technology, 2021, **133**, 106507.

[9] H. Delbarre, C. Przygodzki, M. Tassou, and D. Boucher, “High-precision index measurement in anisotropic crystals using white-light spectral interferometry,” Applied Physics B, 2000, **70**(1), 45-51.

Chapter 2: (C2)

[1] J. Na, H. Y. Choi, E. S. Choi, C. Lee, and B. H. Lee, “Self-referenced spectral interferometry for simultaneous measurements of thickness and refractive index,” Applied Optics, 2009, **48**(13), 2461-2467.

[2] S. J. Park, K. S. Park, Y. H. Kim, and B. H. Lee, “Simultaneous Measurements of Refractive Index and Thickness by Spectral-Domain Low Coherence Interferometry Having Dual Sample Probes,” IEEE Photonics Technology Letters, 2011, **23**(15), 1076-1078.

[3] J. Jin, J. W. Kim, C. S. Kang, J. A. Kim, and T. B. Eom, “Thickness and refractive index measurement of a silicon wafer based on an optical comb,” Optics Express, 2010, **18**(17), 18339-18346.

[4] S. Maeng, J. Park, B. O, and J. Jin, “Uncertainty improvement of geometrical thickness and refractive index measurement of a silicon wafer using a femtosecond pulse laser,” Optics Express, 2012, **20**(11), 12184-12190.

[5] J. Park, J. Jin, J. W. Kim, and J. A. Kim, “Measurement of thickness profile and refractive index variation of a silicon wafer using the optical comb of a femtosecond pulse laser,” Optics Communications, 2013, **305**, 170-174.
[6] J. Park, J. Bae, J. A. Kim, and J. Jin, “Physical thickness and group refractive index measurement of individual layers for double-stacked microstructures using spectral-domain interferometry,” Optics Communications, 2019, **431**, 181-186.
[7] J. Park, H. Mori, and J. Jin, “Simultaneous measurement method of the physical thickness and group refractive index free from a non-measurable range,” Opt. Express, 2019, **27**(17), 24682-24692.

Chapter 3: (C3)

[1] J. Na, H. Y. Choi, E. S. Choi, C. Lee, and B. H. Lee, “Self-referenced spectral interferometry for simultaneous measurements of thickness and refractive index,” Applied Optics, 2009, **48**(13), 2461-2467.
[2] S. J. Park, K. S. Park, Y. H. Kim, and B. H. Lee, “Simultaneous Measurements of Refractive Index and Thickness by Spectral-Domain Low Coherence Interferometry Having Dual Sample Probes,” IEEE Photonics Technology Letters, 2011, **23**(15), 1076-1078.
[3] K. D. Sanjit, and P. K. Mahendra, “Spectrally resolved white–light phase–shifting interference microscopy for thickness–profile measurements of transparent thin film layers on patterned substrates,” Optics Express, 2006, **14**(11), 4662-4667.
[4] K. Joo, and S. Kim, “Absolute distance measurement by dispersive interferometry using a femtosecond pulse laser,” Optics Express, 2006, **14**(13), 4954-4960.
[5] K. Zhang, S. Choi, O. Sasaki, S. Luo, T. Suzuki, Y. Liu, and J. Pu, “Large thickness measurement of glass plates with a spectrally resolved interferometer using variable signal positions,” OSA Continuum, 2021 **6**(4), 1792-1800.
[6] Y. Ghim, H. Rhee, H. Yang, and Y. Lee, “Thin-film thickness profile measurement using a Mirau-type low-coherence interferometer,” Measurement Science and Technology, 2013, **24**(7), 705002.

Chapter 4: (C4)

[1] M. Haruna, M. Ohmi, T. Mitsuyama, H. Tajiri, H. Maruyama, and M. Hashimoto, “Simultaneous measurement of the phase and group indices and the thickness of transparent plates by low-coherence interferometry,” Optics Letters, 1998, **23**(12), 966–968.
[2] S. Kim, J. Na, M. J. Kim, and B. H. Lee, “Simultaneous measurement of refractive index and thickness by combining low-coherence interferometry and confocal optics,” Optics Express, 2008, **16**(8), 5516–5526.

[3] F. Daniel, H. D. Ford, and P. T. Ralph, “Spectrometer-based refractive index and dispersion measurement using low-coherence interferometry with confocal scanning,” Optics Express, 2018, **26**(3), 3604-3617.
[4] C. Sainz, P. Jourdain, R. Escalona, and J. Calatroni, “Real time interferometric measurements of dispersion curves,” Optics Communications, 1995, **110**, 381-390.
[5] D. X. Hammer, A. J. Welch, G. D. Noojin, R. J. Thomas, D. J. Stolarski, and B. A. Rockwell, “Spectrally resolved white-light interferometry for measurement of ocular dispersion,” Journay of the Optical Society of America A, 1999, **16**(9), 2092-2102.
[6] D. J. Bang, Y. Kim, Y. Kim, M. J. Kim, K. H. Kim, “Simultaneous measurement of group and phase refractive indices and physical thickness of transparent plates with low coherence Fabry–Perot interferometry,” Applied Optics, 2018, **57**(16), 4428-4433.
[7] Y. Arosa, and R. Fuente, “Evaluation of group index in spectrally resolved white light interferometry,” Optics & Laser Technology, 2021, **133**, 106507.
[8] H. Delbarre, C. Przygodzki, M. Tassou, and D. Boucher, “High-precision index measurement in anisotropic crystals using white-light spectral interferometry,” Applied Physics B, 2000, **70**(1), 45-51.
[9] Y. Arosa, E. L. Lago, L. M. Varela, and R. Fuente, “Spectrally resolved white light interferometry to measure material dispersion over a wide spectral band in a single acquisition,” Optics Express, 2016, **24**(15), 17303-17312.
[10] J. Na, H. Y. Choi, E. S. Choi, C. Lee, and B. H. Lee, “Self-referenced spectral interferometry for simultaneous measurements of thickness and refractive index,” Applied Optics, 2009, **48**(13), 2461-2467.
[11] J. Jin, J. W. Kim, C. S. Kang, J. A. Kim, and T. B. Eom, “Thickness and refractive index measurement of a silicon wafer based on an optical comb,” Optics Express, 2010, **18**(17), 18339-18346.
[12] S. J. Park, K. S. Park, Y. H. Kim, and B. H. Lee, “Simultaneous measurements of refractive index and thickness by spectral-domain low coherence interferometry having dual sample probes,” IEEE Photonics Technology Letters, 2011, **23**(15), 1076-1078.
[13] S. Maeng, J. Park, O. Byungsung, and J. Jin, “Uncertainty improvement of geometrical thickness and refractive index measurement of a silicon wafer using a femtosecond pulse laser,” Optics Express, 2012, **20**(11), 12184-12190.
[14] J. Park, J. Bae, J. A. Kim, and J. Jin, “Physical thickness and group refractive index measurement of individual layers for double-stacked microstructures using spectral-domain interferometry,” Optics Communications, 2019, **431**, 181-186.
[15] K. N. Joo, and S. W. Kim, “Absolute distance measurement by dispersive interferometry using a femtosecond pulse laser,” Optics Express, 2006, **14**(13), 5954-5960.
[16] K. N. Zhang, S. Choi, O. Sasaki, S. J. Luo, T. Suzuki, Y. X. Liu, and J. X. Pu, “Large thickness measurement of glass plates with a spectrally

resolved interferometer using variable signal positions," OSA Continuum, 2021, **4**(6), 1792-1800.
[17] I. H. Malitson, "Interspecimen Comparison of the Refractive Index of Fused Silica," Journay of the Optical Society of America, 1965, **55**(10), 1205-1209.

LIST OF PUBLICATIONS

1. Kaining Zhang, Osami Sasaki, Samuel Choi, Songjie Luo, Takamasa Suzuki, and Jixiong Pu, "Measurement of phase refractive index directly from phase distributions detected with a spectrally resolved interferometer," Applied Optics, 2021, **60**(31), 10009-10015.

2. Kaining Zhang, Samuel Choi, Osami Sasaki, Songjie Luo, Takamasa Suzuki, Yongxin Liu, and Jixiong Pu, "Large thickness measurement of glass plates with a spectrally resolved interferometer using variable signal positions," OSA Continuum, 2021, **4**(6), 1792-1800.

3. Kaining Zhang, Samuel Choi, Osami Sasaki, Songjie Luo, Takamasa Suzuki, Yongxin Liu, and Jixiong Pu, "Shape measurement of large thickness glass plates with a white-light scanning interferometer using a compensation glass and a fixed reference surface," Engineering Research Express, 2021, **3**(2), 0025044 1-10.

4. Kaining Zhang, Osami Sasaki, Songjie Luo, Takamasa Suzuki, Yongxin Liu, and Jixiong Pu, "A dual-scanning white-light interferometer for exact thickness measurement of a large-thickness glass plate," Measurement Science and Technology, 2020, **31**(4), 045009, 1-5.

5. Kaining Zhang, Samuel Choi, Osami Sasaki, Songjie Luo, Takamasa Suzuki, and Jixiong Pu, "Large thickness measurement of glass plates with a spectrally resolved interferometer using two positions of a reference surface and a compensation glass," Proc. SPIE 11899, Optical Metrology and Inspection for Industrial Applications VIII, 118990A-1～7 (9 November 2021); doi: 0.1117/12.2601233.

ACKNOWLEDGEMENT

I would like to express my sincere gratitude to Prof. Takamasa Suzuki, Prof. Osami Sasaki, and A/Prof. Sameul Choi.

My supervisor Prof. Suzuki gave me a lot of helps on my research and life during my doctoral studies, and these guidance helped me to overcome many difficulties in my doctoral studies.

Prof. Sasaki gave me a lot of guidance on my research during my master studies at Huaqiao University and my doctoral studies. He taught me how I should conduct my research.

A/Prof. Choi taught me experimental skills, and he improved my theoretical and practical understanding of interferometry.

I am grateful to Prof. Jixiong Pu who provided the experimental environment for some of my researches.

I am thankful to my family members. Their support and understanding provided motivation for me to complete my doctoral study.

Finally, I would like to thank the Niigata University. The life and academic atmosphere in the university gave me a deep impression.